

# Appendix F

# **Union Pacific Resources**

## **Stratos Federal #1**

### Logging/Formation Evaluation

*Stan Denoo*

*Schlumberger Denver*

#### **Abstract**

This report covers the wireline formation evaluation for the Union Pacific Resources Stratos Federal 1-24 in Section 24, Township 22N, and Range 107W of Sweetwater County, Wyoming. The analysis was initiated as part of the GRI Greater Green River Basin Production Improvement Project which coincides with the DOE Greater Green River Basin Production Improvement Project. The evaluation starts with the standard triple combo wireline services of Resistivity, Density, and Neutron and continues through to the more complex logs. These include Azimuthal Resistivity Images, Formation Micro Images, Natural Gamma Ray Spectrometry, Accelerator Porosity Sonde, Combinable Magnetic Resonance, and Dipole Shear Images. The formation description becomes more refined as the logging suite becomes more complete. The triple combo logs give porosity, saturation and lithology. Extra logs are needed to address fractures, thin beds, permeability, frac treatment planning and production benchmarking. This refinement must be balanced against increased logging costs and tailored for a specific area.

In summary, there are logs that identify fractures, two logs that show stress orientation, two logs that give resistivity, two ways of computing water saturation, two different neutron porosities, two methods for computing log based permeability and two ways to get measured shear data.

This is a more detailed logging package than typically run by the industry, but this well is in a deep unexplored portion of the Greater Green River Basin and geologic information is minimal. It is also an ideal opportunity to compare most of the current technology that exists today. Unfortunately, this well is not a "classic" good well, so although there are three logs that are capable of detecting fractures, no fractures were detected on the electric logs. Ideal examples from a generic well are used in this report where appropriate to demonstrate points throughout the text. Core data is used to verify the interpretation.

### **Standard Logging Suite**

The well was drilled to a depth of 16,231' with a bit size of 7.875 inches, a bottom hole temperature of 250° F, and a mud weight of 11.4 lbs/gallon. The salinity of the mud required the use of the Dual Laterolog rather than the induction type tools. The Laterolog is composed of a shallow and a deep resistivity, but no very shallow MSFL. The density tool is the standard dual detector Litho-Density with pef curve. The Neutron is the two detector compensated thermal neutron recorded on a sandstone matrix. The Gamma Ray, caliper, and delta rho were also included as part of the standard suite. An SP would have been unusable due to mud conditions.

### **Triple Combo theory**

The Gamma Ray is a recording of the natural formation radioactivity. Clay minerals are usually radioactive while other minerals are not. Thus the Gamma Ray is a good, but not a perfect shale indicator. For resistivity, the Dual Laterolog was run. With the Deep Laterolog, the survey current,  $i_o$ , is forced horizontally into the formation in the shape of a current sheet with a constant thickness within the radius of the sonde. Both the  $i_o$  and the bucking current are returned to the electrode at the surface. With the Shallow Laterolog the bucking current returns to the far end electrodes of the sonde and the  $i_o$  current remains a constant thickness for only a short distance. For porosity, the Density and Neutron are used. The Gamma Rays emitted by a radioactive Cesium 137 source lose energy and are scattered through collisions with the electrons in the formations through Compton scattering. The number of scattered electrons per unit volume that reach the detectors depends on the Bulk Density of the formation. By counting the number of Gamma Rays in the lower energy region (photoelectric effect) and the high energy region (Compton scattering), the photoelectric absorption index is determined and from this, the Pef curve is produced. Fast neutrons emitted from a radioactive Neutron source are scattered and slowed by collisions with the nuclei of the formation. Hydrogen plays the predominate role in slowing down neutrons. Some time after reaching the thermal level of energy the neutrons are captured by the nucleus and Gamma Rays of capture are emitted. Near and far detectors collect

these count rates. These counts are converted to sandstone, limestone, or dolomite Neutron porosity

### **Interpretation Model**

The Dual Water Model is used for saturation analysis. This is based on the classic Archie water saturation determination. Compensation for shale in the model is done through the use of the mixed  $R_w$  and the introduction of total and effective porosity. The water resistivity is a mixture of free water and bound shale water. The more shale, the larger the percentage of shale water that is used in the  $R_w$  term. This model needs formation resistivity, bound water saturation, free and bound water resistivity, and total porosity. The Deep Laterolog was taken as  $R_t$ . Correction of  $R_t$  for filtrate invasion was not an issue. The bound water saturation for the model was determined from the minimum of Gamma Ray, Neutron,  $R_{hg}$ , and  $U_{ma}$ . A linear transform was used on all the bound water indicator. The end points were determined through use of appropriate crossplots. Total porosity is from the standard density neutron crossplot (Figure 1) with a light hydrocarbon correction applied where appropriate. The effective porosity is functioned from the total porosity and bound water saturation. A linear transform with zero percent effective porosity in pure 100% bound water shales and effective equal to total porosity in 0 % shale intervals has been used.  $R_w$  values were taken from a catalog.

The lithology was computed using the  $U_{ma}$  and  $R_{hg}$  crossplot (Figure 2). This technique uses bulk density, neutron porosity and  $P_{ef}$  to compute the non-shale porosity free matrix volumes in combinations of three lithologies. The clay volume from the bound water saturation is then added to the three mineral analysis for the final results.

The formation analysis result is shown in Figure 3. Track 1 contains the Gamma Ray and caliper, track 2 has the Laterolog deep and shallow resistivities. Track 3 is the computed lithology including porosity and fluid analysis. The sandstone contains a small amount of carbonate cement. The shale is assumed to be predominately illite. Track 4 is the porosity on an expanded 0 to 25 % scale. Hydrocarbon and water volumes are shown with the effective and total porosity. The computed total porosity goes from a solid coding to a dashed coding on the display whenever the bad hole logic of the evaluation program is being used. The software package used in the evaluation is the linear sequential Formation Evaluation Summary engine of GeoFrame.

## **The Reservoir**

The Frontier sands begin with a fining upward sequence from 16,080' to the shale break at 16,032' with two other sand bodies from 16,030-16,018' and 16,006-15,995'. The shale from 16,018-16,006' is a severe washout that affects all the logs especially the porosity logs. Maximum porosity is 11.5%. Only a few several hundred feet above and below the Frontier sandstone have been analyzed in this report.

A log analyst with experience in the area will notice that below 16,557', the resistivities are low and constant, and almost independent of porosity. This same signature is found in some of the marine Frontier sections of southwestern Wyoming and is indicative of a reworked sediment that has no visible bedding planes and has experienced a redistributing of the shale grains. An evaluation with the standard logging suite for water saturation and neutron density gas crossover may be misleading due to the possible redistribution of shale. In these intervals porosity may or may not be preserved and some uncharacteristically good wells can result. This may or may not be the case for the Stratos Fed 1-24 well.

The next results (Figure 4) are tracks 3 and 4 of the previous figure with the addition of a water saturation track. Core porosity has been added in track 4 as little open squares. The core water saturations are the solid boxes shown in the far right hand track. The match between the core porosity and the computed total porosity was good and required no modification from the first pass. This match infers that the computed lithology is very close and, short of x-ray defraction results, the computed lithologies will be used as is. The volume of bound water and shale may be lightly overestimated in the bottom portion of the Frontier section, but this does not affect the final results.

The saturation match to core on the right side of Figure 4 is, however, not very good and will require further refinement. Normally the core water saturation must be used with caution, but in this case due to the low porosity, low permeability, little or no invasion, and the good core handling techniques the core saturation results can be used. The original water saturations were computed with the cementation exponent of 2.0 and water resistivities of 0.10 ohm-meters, free, and 0.12 ohm-meters, bound, at bottom hole temperature. These starting points are taken from a Frontier sandstone's data base for southwestern Wyoming. The final results were obtained with

water values of 0.07 ohm-meters, free, and 0.075 ohm-meters, bound, and cementation exponent of 1.8 (Figure 5). The saturation exponent was left at 2.00. These results were obtained by trial and error guided by  $r_{wa}$ - $s_{wb}$  crossplots since no 100% water zone was available. The matching of the core water saturation can be used in other tight gas basins to determine water salinity in intervals that normally do not produce water. The correct water saturation is needed to calculate the relative insitu permeability.

Good control on lithology, porosity, and fluid saturations has been verified by core analysis. This is as technical as standard log interpretation and formation evaluation can be exploited with the triple combo logging suites. Log derived permeability is not presented here due to the suspected geologic alterations that may have destroyed any porosity - permeability relationship of the reservoir. No inference of fractures can be made at this time with the logging data discussed so far. Neither can evaluation of thin beds, bound and free porosity, stress orientation, and mechanical properties be discussed.

### **Hi Tech ARI**

The first of the new technologies to be covered is the Azimuthal Resistivity Imager. This tool was designed as the next generation Laterolog. The Azimuthal Imager is basically a high powered, advanced dual Laterolog. It makes 12 deep and 12 shallow resistivity measurements in 30° segments around the borehole. These images have a six inch vertical resolution compared to the Dual Laterolog resolution of about two feet. Data sampling is 12 times per foot compared to two times per foot for the standard Dual Laterologs. Figure 6 is an example of an ARI presentation of the 12 azimuthal curves and the Ild and IIs from a different well in the Rocky Mountain Region. The ARI signature in fractures is found above 10,360' in the circle. Two azimuthal curves read low and they do not have the same "shape" as the others. In fact, they are flatter and lazier. These are the two segments that are reading in the fracture. The other ten are reading the matrix. The FMI image on the left side shows the fracture. The slight offset of the twelve peaks can also be used to determine the structural dip when recorded with the appropriate inclinometry data. The detail is too poor for stratigraphic dips, but is sufficient for structural dip. A computed electronic caliper from the 12 arrays can also be extracted from the data. Now compare the ARI from the Stratos Federal 1-24 well in Figure 7. Only the minimum and maximum of the twelve resistivities are presented with the Ild and IIs. No obvious fracture signature can be seen. In fact, very little electrical anisotropy can be seen. Each of the 12 Deep Laterologs read very close to each other except in the very tight regions. From this we can infer

the lack of natural fractures, low formation dips, and the presence of thin beds. Use of the median resistivity for water saturation made only a small difference due to the symmetry of the reservoir and the lack of a high resolution porosity. The dip and caliper computations were not done due to the lack of a recorded inclinometry.

### **Hi Tech FMI**

The 192 microresistivity buttons of the Formation Micro Imager recorded at 120 samples per foot provide the most complete detailed borehole imaging available without actually coring the formation. Analysis of these images in Figure 8 confirms the azimuthal resistivity interpretation of no fractures, low dips, and many thin beds. At this hole size approximately 90% of the borehole is covered with the FMI and the extended pads.

The FMI in Figure 9 and the ARI in Figure 10 confirms reworking of the lower Frontier. This reworking is seen as a lack of bedding planes below 16,557'. The degree of reworking and the effects of the reworked clays on the resistivities can not be quantified. No faults or changes in formation dip are indicated. No stratigraphic analysis of this log was done.

Further study on the Image Examiner of the FMI image suggests a fluvial environment in the upper Frontier sections above 16,032' and marine deposition in the lower half of the Frontier. See the core description in the main discussion for further information (Figure 3-2).

### **Borehole Geometry**

Another piece of technology that the FMI brings is borehole geometry in the form of an oriented four arm caliper, and its correlation to the principle horizontal stress direction. Borehole elongations in the absence of natural fractures puts the long axis of the borehole perpendicular to the maximum horizontal stress due to the high tangential stresses at the borehole wall. This is also the azimuthal direction of an induced hydraulic frac. In the presence of natural fractures, the long axis of the borehole will be parallel to the natural fractures and the induced fractures due to breakouts around the fracture tip near the borehole wall. Borehole breakout data for the Stratos #1-24, with its apparent lack of natural fractures, indicates that the principle horizontal stress is oriented in a NE-SW direction. Figure 11 is a summation of each recorded caliper depth from 16,200' to 15,800'. The round circle is bit size. Readings less than bit size are found inside the circle and caliper readings greater than bit size are outside the circle. This is not a strong

directional trend and should be used with a bit of uncertainty. An argument for either NW or NE can be made, but the dominant trend seems to be NE. The four traces moving out from the center of the plot are the calipers opening up at the beginning of the log.

Borehole geometry in this type of reservoir is better suited to the borehole televiewer type of measurement with a rotating image that takes a caliper reading every 5 degrees of azimuth. Caliper images are enhanced, but formation images are diffused, compared to the FMI. Figures 12a and 12b are examples from a different well using UBI calipers showing some subtle stress differences that are invisible to other types of calipers. In part A of the picture, the borehole is being shoved in very slightly from the NW at a depth of 15,336.366' and in part B of the figure, the borehole has slipped perpendicular to the applied stress just 0.049 feet further up the hole. The principle stress is from the NW and the release of stress is perpendicular to that.

### **Hi Tech HNGS**

Like the Gamma Ray, the **H**igh resolution **N**atural **G**amma Ray Spectrometry log measures the natural radioactivity of the formation, but unlike the GR which measures the total radioactivity, the HNGS measures the number of gamma rays and the energy level of each. The outputs are calibrated concentrations of Potassium, Thorium, and Uranium, a regular Gamma Ray and a Uranium corrected Gamma Ray. The HNGS outputs were crossplotted similar to Figure 13 and Figure 14 for clay identification in the Frontier section, but the results were inconclusive. Mixed layer and illite clays were the dominant clays. Uranium was not dominant in the Gamma Ray Spectrum. The corrected Gamma Ray was used to enhance clay volume in the formation evaluation.

### **Hi Tech APS**

The next log in the hi tech suite is the **A**ccelerator **P**orosity **S**onde, the next generation Neutron. Compared to the standard Compensated Neutron Log that uses a chemical source and two thermal detectors, this neutron device uses an electronic neutron generator and five epithermal detector arrays. This produces porosity measurements at different depths of invasion and neutrons with a smaller shale response than thermal neutrons and Sigma capture cross section. Near borehole porosity, STOF, is approximately 6 inches from the borehole. APSC is next at about 12 inches, and the FPSC is taken from an area 18 inches from the borehole wall. For comparison, the APSC Neutron is plotted with the Density and CNL porosities in Figure 15. In the shaly lower section of the Frontier, the APSC reads less than CNL primarily because of the

epithermal/thermal differences. In the marine section of the Frontier, the APSC and CNL are very close. But in the fluvial section, the CNL is seeing more gas than the APSC. An invasion profile involving the different neutrons is shown in Figure 15. Darker, cold blue colors are water, while lighter, hot colors are gas. The borehole is at the right and 24 inch invasion is at the left edge of track. Starting near the borehole is the Sxo from Sigma, then the saturation from the STOF/PHIT algorithm, then the APSC/PHIT, the FPSC/PHIT gas saturation and finally CNL/PHIT. This visually suggests that more gas is near the borehole than two feet deep into the Lower Frontier and an annulus of water is present in the upper section. All this points towards poor filtrate invasion and less than optimum conditions for permeability and good gas production. The APS has the added advantage of having a different name for each lithology type. APSC is Accelerator Porosity Sandstone Corrected while its counterpart is APLC and APDC for Limestone Corrected and Dolomite Corrected.

The APS also has a Sigma measurement obtained by the rate of decay of the epithermal neutrons in much the same way as TDT family of cased hole tools. Sigma can produce a flushed zone saturation independent of the m and n variables used in an Archie based analysis. Sigma from the APS and its Sxo was used to verify the cementation exponent of 1.8 used for the water saturation calculations in this report. Sxo from Sigma was set equal to Sxo from the Dual Water model and m was back-calculated from IIs, phit, and Rmf.

### **Hi Tech CMR**

The next hi tech service is the Combinable Magnetic Resonance. The NMR signal originates from the hydrogen nuclei in the pore fluids much like the CNL, but the similarity ends there. The CMR measures the precession of hydrogen after the application of the proper magnetic field sequences. The two measurements made by the CMR relate to the effective porosity and the pore size (T2). The recorded effective porosity is further refined into the free and capillary bound porosity. A five minute CMR station, Figure 16, was taken at 16,550' and recorded an effective porosity of 8.2 pu. The effective porosity is the total area under the T2 distribution curve. The capillary bound fluid is the area to the left of the 33 msec line and the free producible fluids are to the right of the cutoff. The shape of the curve relates to the pore distribution and permeability. The addition of the CMR porosity to the analysis of Figure 17 indicates that only small amounts of free water are suspected from the Frontier interval. The hydrocarbon and bulk volume water in the middle track have the addition of bound and moveable fluids. Subtracting the bound fluids and the gas filled porosity from the effective porosity leaves the producible water, which while

not zero, is only about 2% of the rock's total volume. The righthand track of Figure 17 shows the CMR porosity with the other porosities. The CMR is the lowest reading of all the porosities. In an ideal case, the CMR porosity should read very close to NPHI in gas reservoirs and it does in a few spots. In the main interval, the CMR porosity reads less than the CNL suggesting either incomplete polarization of the hydrogen gas due to logging too fast, or an abundance of very fine grained material. The recorded station indicates incomplete polarization on the continuous pass. Producibility of the reservoir should not be a problem based on comparing the CMR and CNL porosities. In very tight gas sands with little or no filtrate invasion, the CMR, which has a depth of investigation of only about 1 inch, will see all gas and reads very low. Hence, very tight gas sands have poor flushing and are very poor reservoirs.

### **Permeability**

The T2 distribution from the CMR shown in Figure 18 represents the pore size distribution. Small pores are to the left and large pores are to the right. The 33 msec line is the cutoff between commercial and non-commercial pore sizes for sandstones. This distribution shows a predominance of fine to very fine pores. The T2 distribution display is absent when hole rugosity makes the T2 distribution dominated by the mud signal. Permeability computed from T2 and gas corrected porosity is shown in the middle track. This is the data with the area codings. The correlation to core data from the CMR was unshifted from the standard algorithm and required no parameter adjustment. A crossplot of porosity to perm algorithm was also computed and is shown as the dark log curve without area shading. These matches, while not "letter perfect", are pragmatically close enough to be useful in the frac design. The small numbers in the depth track of Figure 18 are the integrated permeability values.

A correlation from the CMR permeability to reservoir insitu permeability was implemented from the simple algorithm that cut the permeability by a factor of 10 for use in the insitu model. This model is very empirical and is only applied to permeabilities of less than one millidarcy. Below 1 md, the square root of permeability is used until the factor of ten is obtained. As simple as it is, it does appear to give the correct order of magnitude to the permeability. The ten factor was based on Swirr and Sw. A more sophisticated approach is under development. The CMR was still in field test during the time of logging. Integrating the CMR insitu permeability over the Frontier, produced 0.075 md ft. Using an estimated reservoir pressure of 12500 psi, Darcy's pseudo steady state radial flow estimates the production benchmark at 25 mcf/day natural and only 46 mcf after a medium size frac with a -4 skin (Figure 19).

## **Hi Tech DSI**

The Dipole Sonic Imager is the last piece of hi-tech logging to be discussed. Two of the possible five modes of sonic acquisition were recorded - a monopole mode and a cross dipole mode. The monopole mode uses a standard, unidirectional source to produce a Compressional and Shear travel time. The travel times are limited by the speed of the borehole fluid. Semblance processing across the eight arrays is used to determine the appropriate travel times. In the cross dipole mode, two directional transmitters, ninety degrees apart are fired sequentially and waveforms are recorded both in and out of phase with the transmitters. The data from Both Crossed Receivers is used to compute shear wave anisotropy in both the travel time and the energy planes.

## **Mechanical Properties DSI**

The compressional data from the monopole, the fast shear from the anisotropy process of the crossed dipole mode, and the bulk density were used to compute the mechanical properties using the Impact program on GeoFrame. Previous monopole acoustic logs could not get reliable shear values in the many marine shales throughout the Rocky Mountain Region. This resulted in unreliable Poisson's ratios. This is not so any more because the Dipole shear is able to acquire good shear values in all types of rocks. Poisson's ratio, Young's Modulus, Bulk Compressibility and Shear Modulus are computed using standard algorithms for every six inch data sample. Data quality in the Stratos 1-24 was less than optimal due to tool sticking and the severe washouts in some of the shales.

The Mechanical Properties and the poroelastic strain model of Impact was used to compute the far field stresses. The results are shown in Figures 20a and 20b. Microstrains of  $0.05 \times 10^{-3}$  and  $0.15 \times 10^{-3}$  were used in the computation for the x and y components. These are values taken from nearby Moxa Arch. This is an overpressured reservoir and pore pressure is a key factor in defining the stress magnitudes. Three mini-frac closure tests were used to verify the stress computations, one below, one in, and one above the zone of interest. The test in the sand was inconclusive, so complete verification was impossible. The stress analysis show very high frac gradients with only a small amount of vertical containment. The straight lines in Young's Modulus, minimum horizontal stress, and Poisson's ratio are the results of zoning the reservoir into twenty layers for input into a 3D frac simulators such as FracCade. Young's Modulus and Poisson's ratio were converted to static moduli before zoning. The dots in tract 2 on the two figures are the closure stresses from the mini-frac. Approximately 1700 psi stress difference

between the sand and shales can be used for frac containment. As the reservoir pressure declines, the stress contrast will increase. The high minimum horizontal stresses may suggest plastic creep, minimum differences between the three major stress tensors, or a lack of a strong principle stress direction. The maximum horizontal stress is greater than the overburden stress.

### **Shear Anisotropy**

Shear waves have vastly different signatures with and without fractures. Anisotropy means the rock properties change with the azimuth around the borehole. The BCR techniques record both shear waves differences and the direction of the disturbance. The recording of the cross dipole mode produces two in-line and two off-line waveforms for each of the 8 receivers for a total of 32 waveforms every six inches of tool travel. These waveforms are paired on equal depth frames and processed with the Both Cross Receiver four component rotation software. The computed results give acoustic anisotropy in time and energy and the direction of the fast shear travel time. Fractures produce a dramatic difference in the minimum and maximum off-line energy and a separation in the fast and slow shear times. Figure 21 is an example of Anisotropy processing in a zone of confirmed fractures. This example is **not** from the Stratos 1-24, but is presented to show what the product looks like. Good separation in the minimum and maximum energy as shown in the depth track. Good, fast shear directional stability is shown in track 2. It is also the angle of the maximum horizontal far field stress and the direction of the induced fractures. Good, fast and slow shear anisotropy are shown in track 3, and good waveform separation is shown in track 4. All of these are signs of fractures and shear anisotropy in the example well. Figure 22 is the results of the shear processing for the Stratos 1-24 well. Very little off-line energy difference, very little waveform separation, and very little travel time difference between the fast and the slow indicate that very little acoustic anisotropy is present in the Frontier section of this well. This lack of anisotropy may explain the paucity of natural fractures or steep formation dips. A summary plot, Figure 23, shows the anisotropy direction without discrimination for data quality and noise. The trend on the plot is in the NE-SW quadrant with a great deal of variability. The direction of the anisotropy is of little value when there is very little anisotropy present.

### **Conclusions / Summary**

This well is not the ideal platform to demonstrate a high tech logging suite due to the lack of character in this reservoir. At this range of porosity, it is necessary to have natural fractures to help with production and this well does not appear to have near borehole fractures. There are also indications that the environment is not conducive to natural fractures.

Porosity, lithology and water saturation were obtained from the standard logging suite. Core data was used to provide the  $R_w$  and  $m$  values. Sigma from the APS gave a similar  $S_w$  with the variable  $m$  technique without the need of core data.

The triple combo can be efficiently upgraded with the ARI to replace the Dual Laterolog. This log adds the measurement of structural dip and electrical anisotropy which can be interpreted as fractures in the correct conditions. For mud systems that must use induction logs, the AIT with its five deep readings of resistivity makes a good flushing estimate, but can provide no fracture data.

A cased hole alternative to the triple combo is the **Thermal Decay Time**. A presentation very similar to Figure 3 can be produced using the TDT Sigma, TDTP porosity, and Gamma Ray. The TDT can eliminate open hole logging for development wells when good control is available. A cased hole TDT was not run on this well, but an APS Sigma, APSC, and GR presentation similar to Figure 3 was produced.

Fractures- or lack thereof, have been verified by the ARI, FMI, and DSI. Any one of these tools would have been sufficient to document natural fractures in this wellbore. Fracture orientation would have been possible with any of the three tools.

The maximum horizontal stress direction was interpreted to be NE-SW from FMI caliper and DSI. Both cross receivers. Some evidence of a NW trend may be interpreted on a few caliper points. No drilling induced fractures were found in this section. The uphole shales did have drilling induced fractures, but these could not be extrapolated to the Frontier.

Low permeability with poor invasion were indicated by the CMR and Neutron-Density and qualitatively from the APS neutron profile. The CMR takes the guesswork out of the porosity to permeability relationship in any type of mud system. It does this by adding the pore size distribution.

An In situ Perm multiplier from the CMR Swirr and the  $S_w$  from the triple combo was used to estimate the real downhole permeability. This is still very much experimental, but was needed for benchmarking.

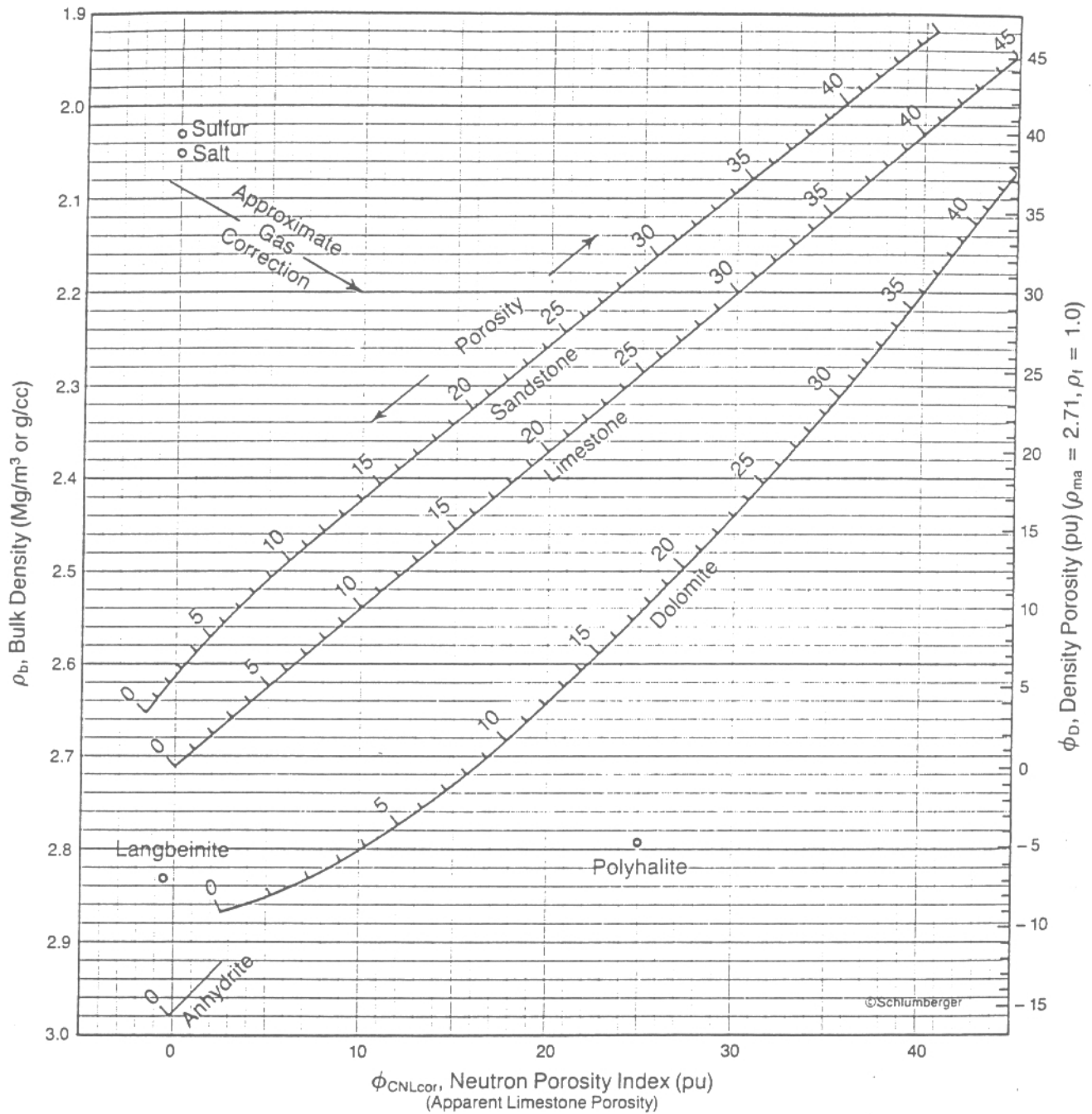
The stress Profile and rock mechanics from the DSI and Bulk Density Pore pressure was the driving factor in this overpressured reservoir. The only tool capable of establishing good rock mechanics is the DSI because the Dipole Shear can measure shear travel times faster than the fluid speed. There are many cases where the Poisson's ratio computed from lithology matches the DSI very well. It is, therefore, possible to get good rock mechanics information without running a sonic log when good well control exists. One of the keys to watch is the shale resistivity. Slight changes in shale  $R_t$  between wells means that the shale Poisson's ratio is also changing and the lithology modeling may be in error.

Benchmarking was part of this project because the goal of any log interpretation should be to optimize production. This can take on many forms. One of the most important and most difficult is to model production. Reliable data for porosity, saturation, permeability, reservoir pressure, and fluid properties are needed. Analysis of the Stratos Federal #1 yielded solid data for all of these parameters, and a benchmark estimation of the base flow rate was possible.

This has been a step by step analysis of a reservoir from the simple to the complex. The interpretations and inferences made are based on the log data and the experience of the logging company representative. The exact details, equations and supporting documentation for this specific report are available from local sources and will not be listed here.

Fresh Water, Liquid-Filled Holes  $\rho_f = 1.0$

For CNL Curves Labeled "NPHI"



EXAMPLE:  $\rho_b = 2.43 \text{ g/cc (or Mg/m}^3\text{)}$   
 $\phi_{\text{CNL}} = 23 \text{ pu (apparent limestone porosity)}$   
 $\rho_f = 1.0 \text{ g/cc (or Mg/m}^3\text{)}$

Plotting on Chart CP-1 indicates the rock to be a limestone-dolomite mixture (approximately 50% limestone, 50% dolomite) or a cherty dolomite (approximately 35% quartz, 65% dolomite). In either case, porosity is about 20 pu.

\*Mark of Schlumberger

CP-1c

Figure 1. Porosity and lithology determination from Formation Density Log and CNL Compensated Neutron Log (Schlumberger Chart Book 1984, Chart CP-1c).

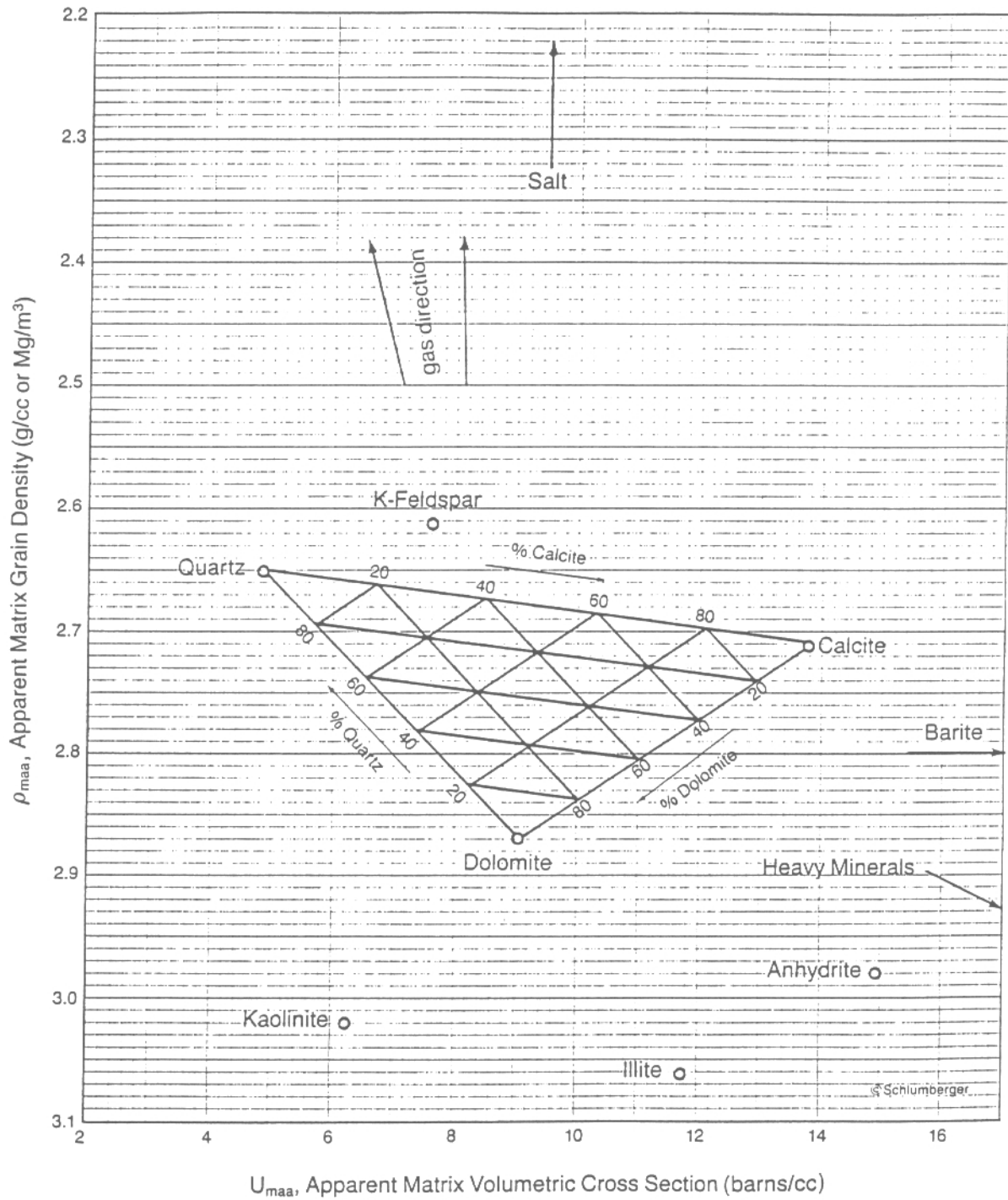
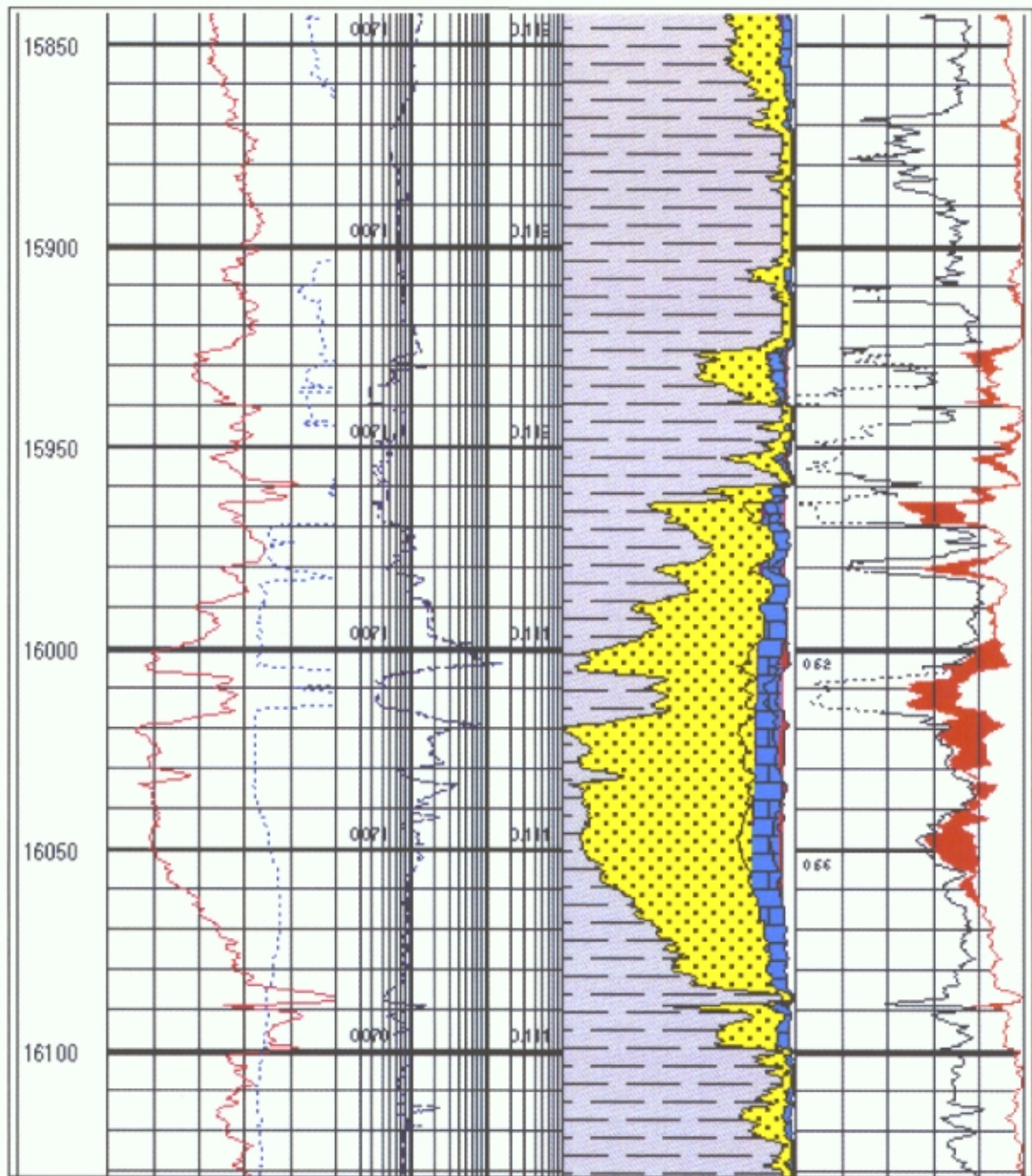
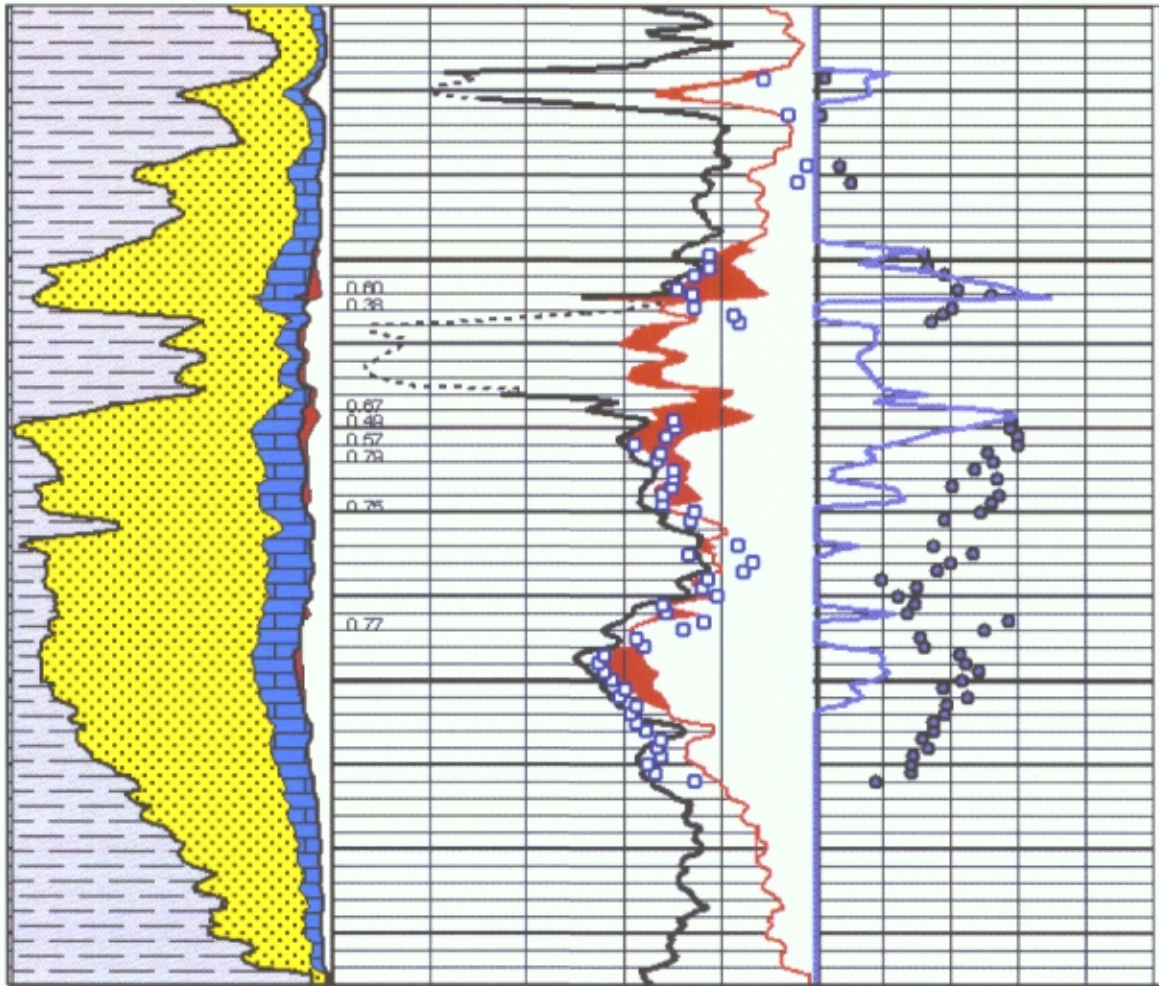


Figure 2. Matrix identification plot (Schlumberger Chart Book - 1984, Chart CP-21).



**Figure 3.** Formation Evaluation Summary using the Dual Laterolog, Density, and Neutron. Track 1 is Gamma Ray and Caliper. Track 2 is LLS and LLD. Numbers 1-1000 in Track 2 are the free and bound water resistivities. Track 3 is Lithology, and Track 4 is 25% Total porosity, Effective Porosity, and Bulk Volume Water. The numbers in Track 4 are the computed water saturations.



**Figure 4.** Core comparisons with Porosity and Water Saturations using  $R_w$  0.10 and  $m = 2$ . Lithology, porosity, and water saturation. Small squares are core data. Small numbers are water saturations.



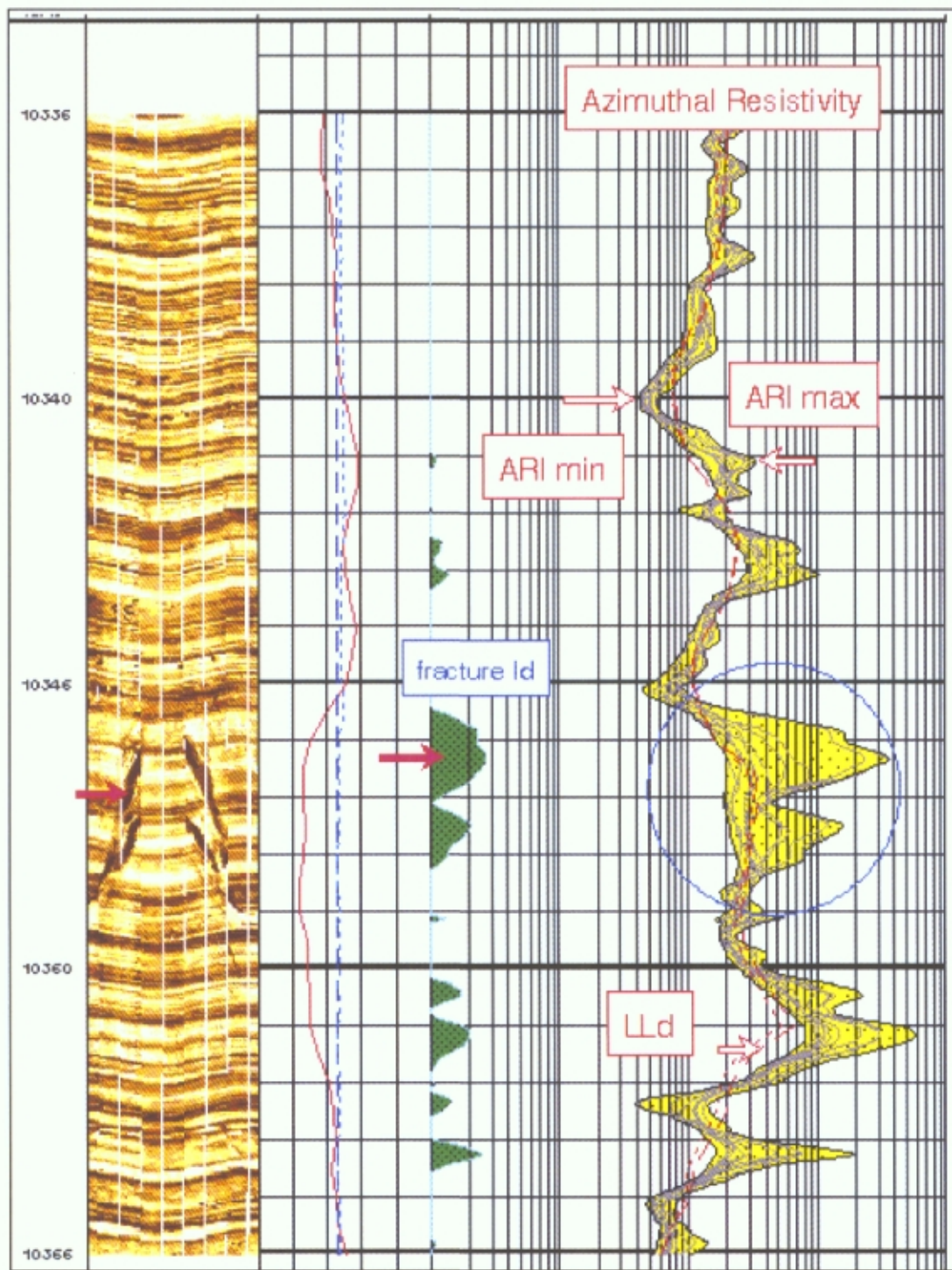


**Figure 6.** ARI Response in Fracture with FMI (Not From This Well). Track 1 is FMI image. Track 2 is GR and Caliper. Track 3 is 12 ARI Resistivities and LLD and LLS.

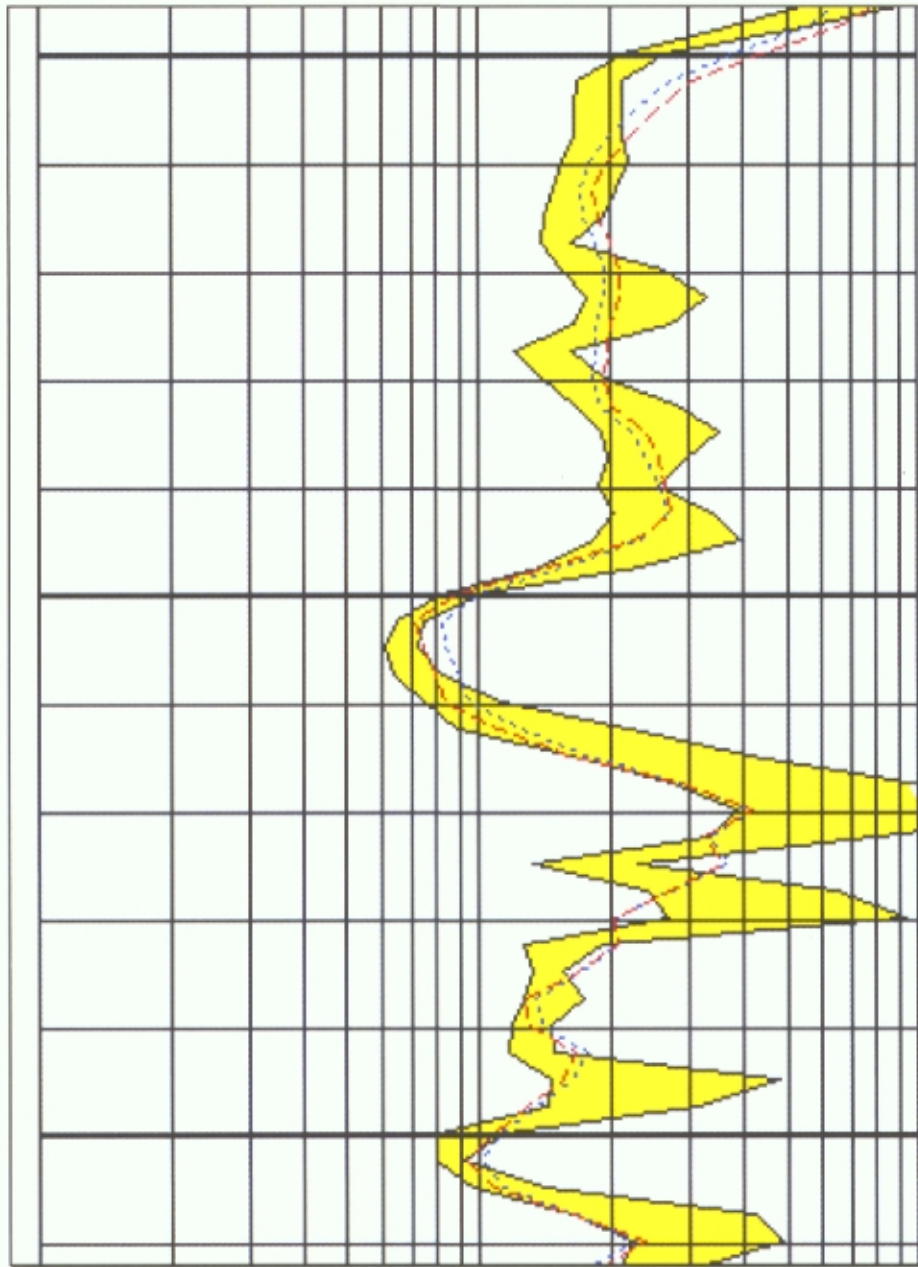


**Figure 7.** ARI response in the upper frontier section. Coding between the minimum and maximum ARI Resistivity. The LLS and LLD are two dotted curves. Notice the better vertical resolution of the ARI. Heavy line in the middle is 16030 ft.

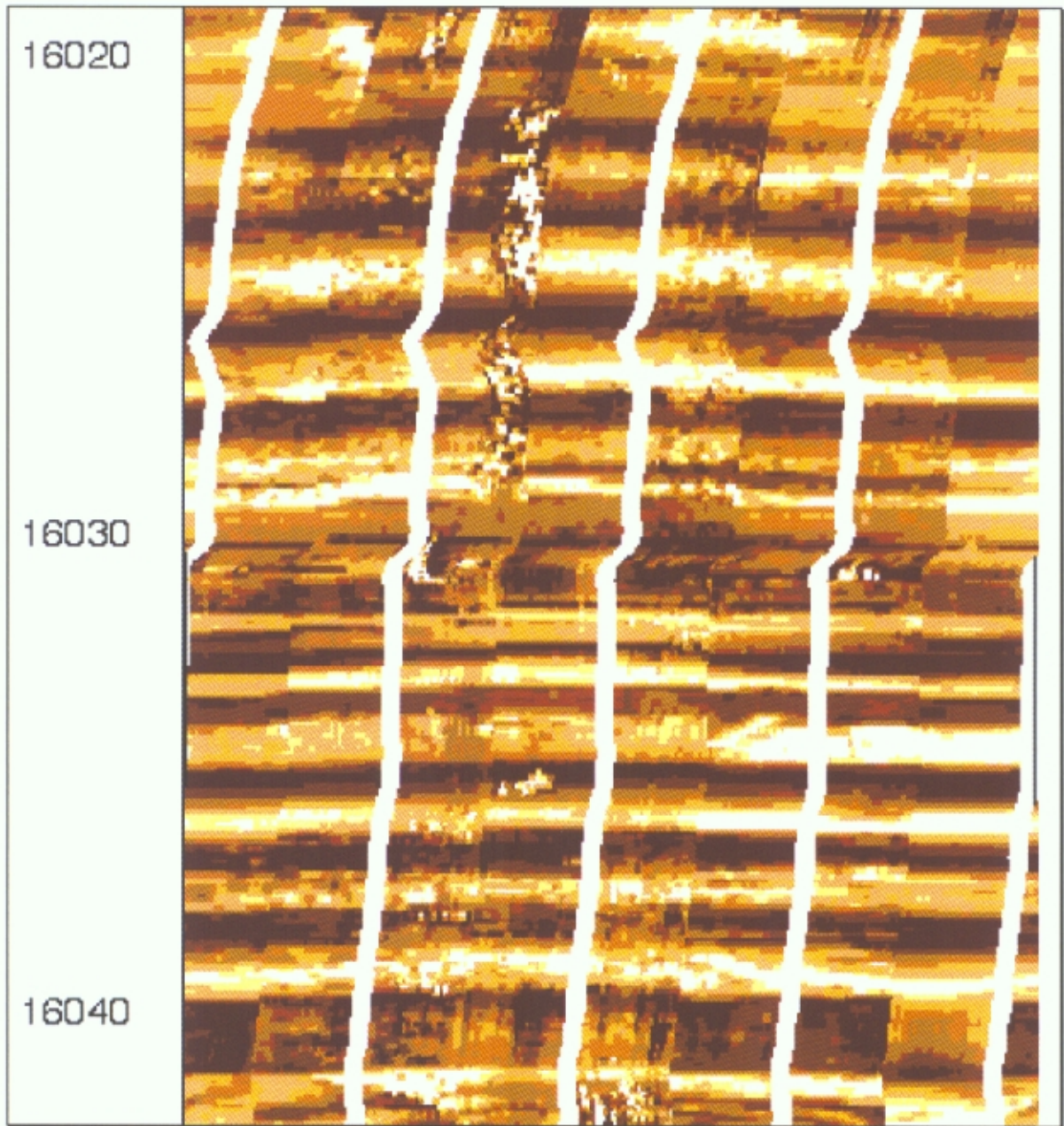


**Figure 8.** FMI in the upper Frontier. Thin Beds, flat dips and no fractures.

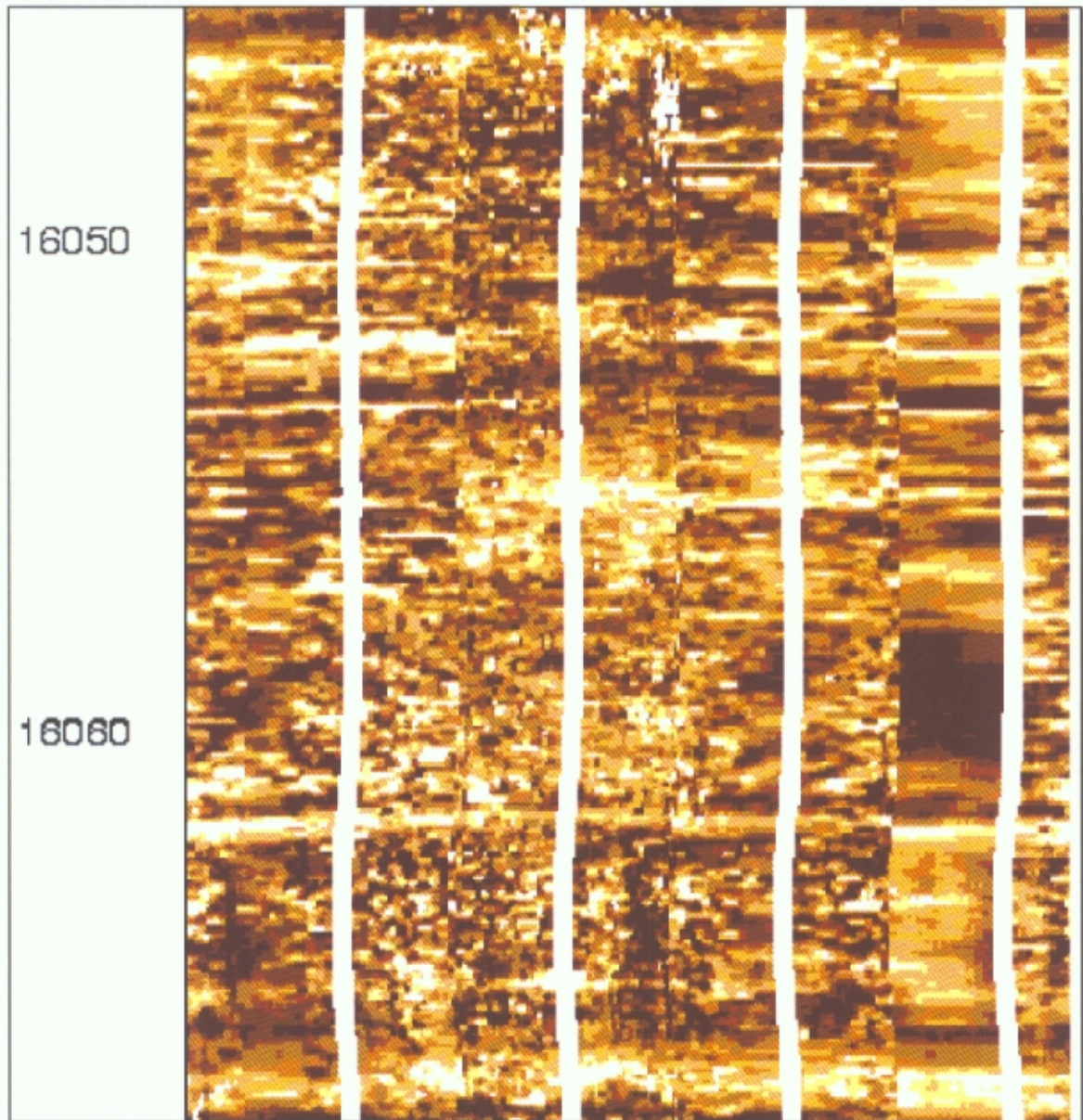


**Figure 9.** FMI in the lower Frontier. Notice the lack of bedding planes. Pad near right edge is noisy due to excessive mud buildup.

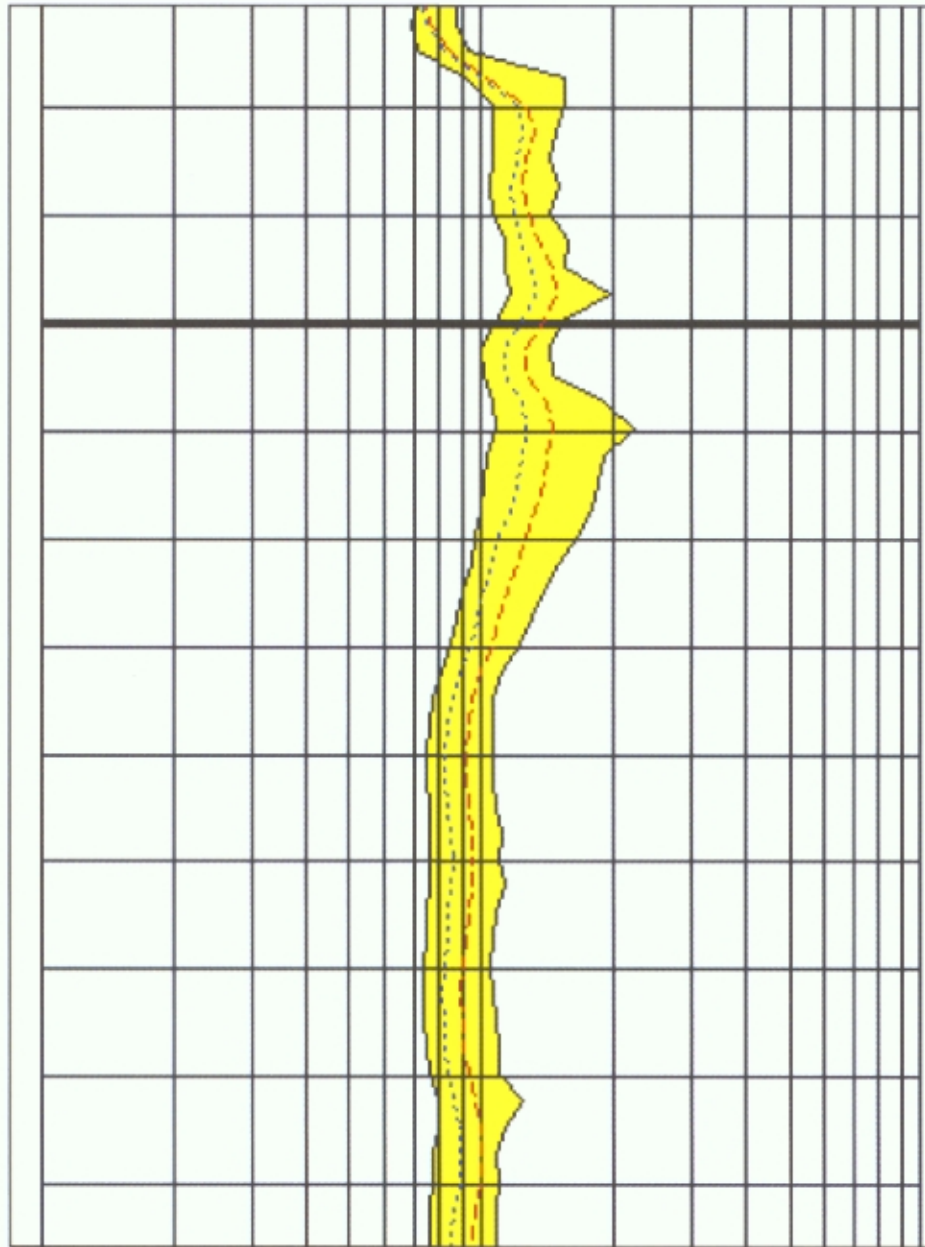


**Figure 10.** ARI in the lower Frontier section. The ARI minimum and maximum resistivity of the 12 data channels are inner and outer solid traces. LLS is dotted and LLD is dashed. Heavy line is 16550 ft.

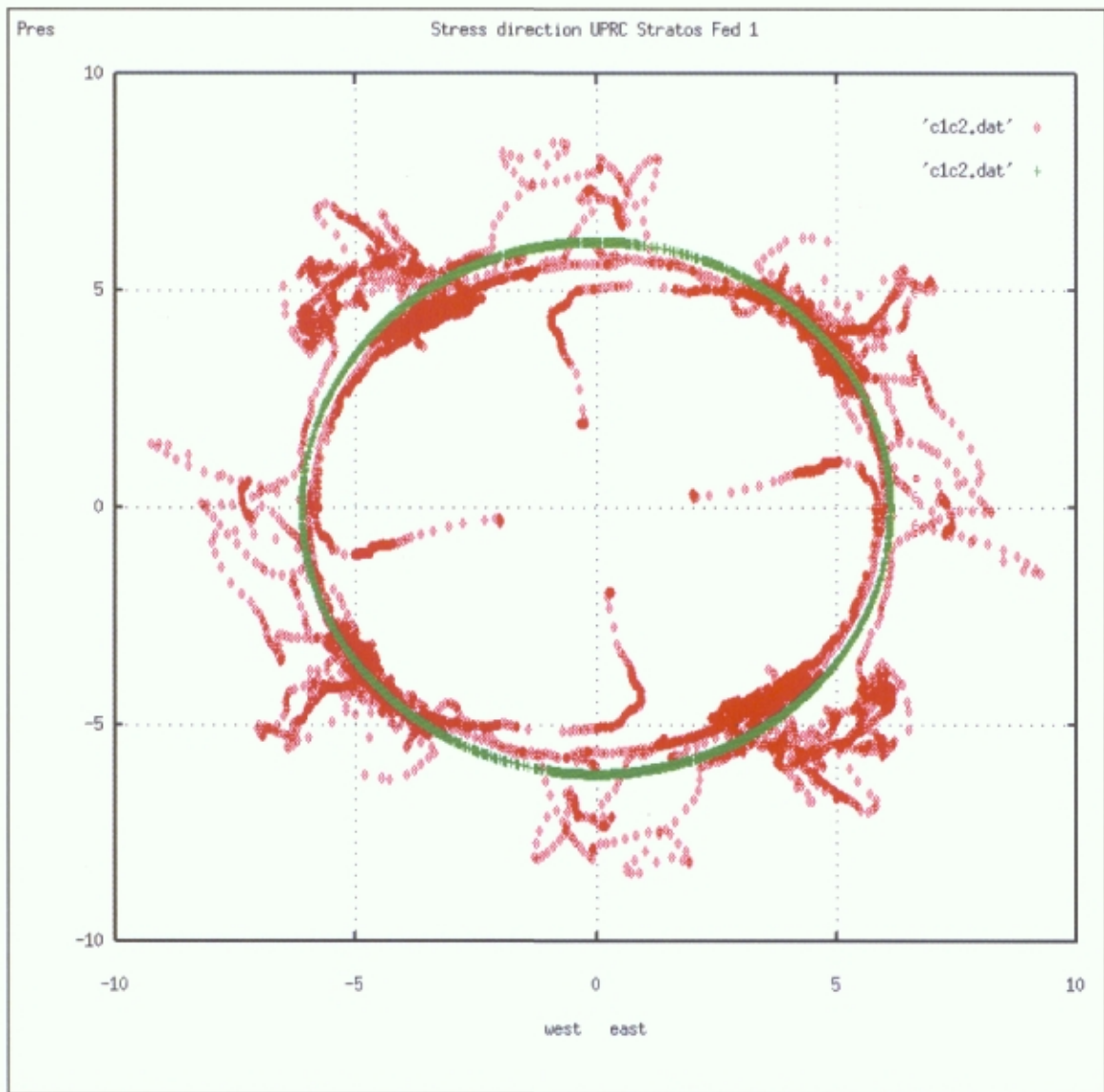


**Figure 11.** Borehole ovality from FMI caliper. North is at the top. NE-SW Stress direction perpendicular to the washouts.

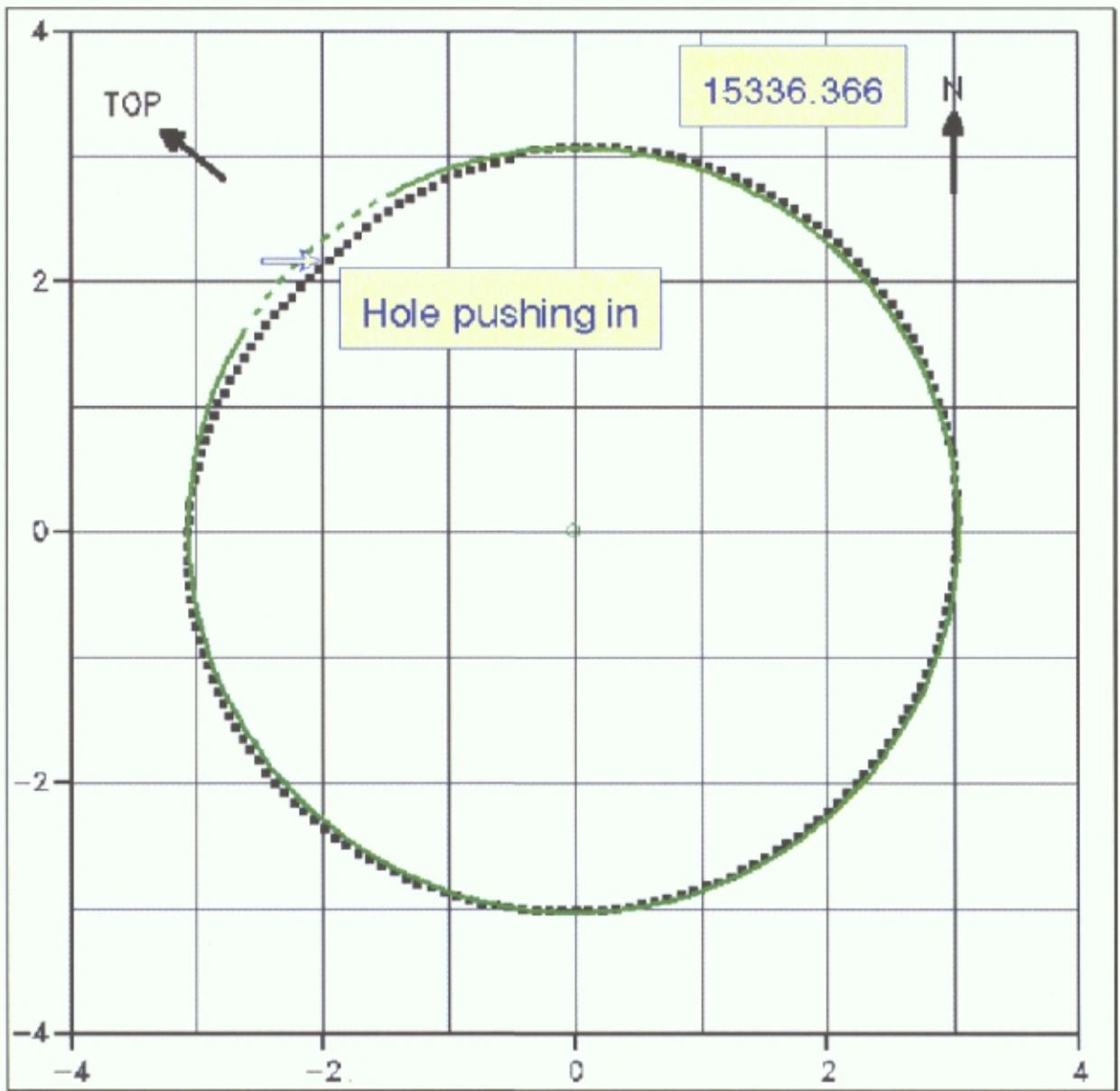


Figure 12a. UBI Example of Hole being pushing in by strong tectonic force.

(Not from this well)

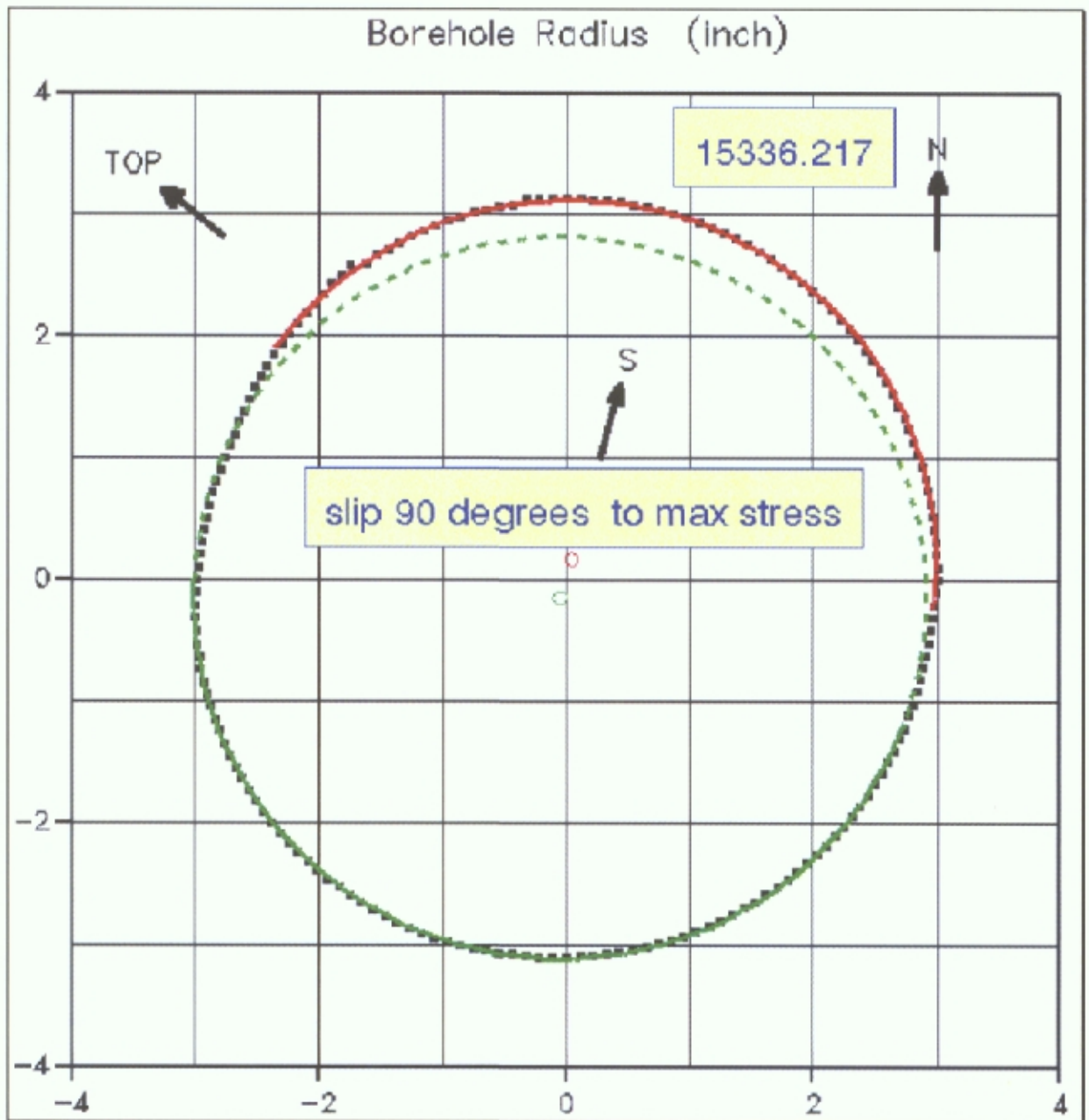
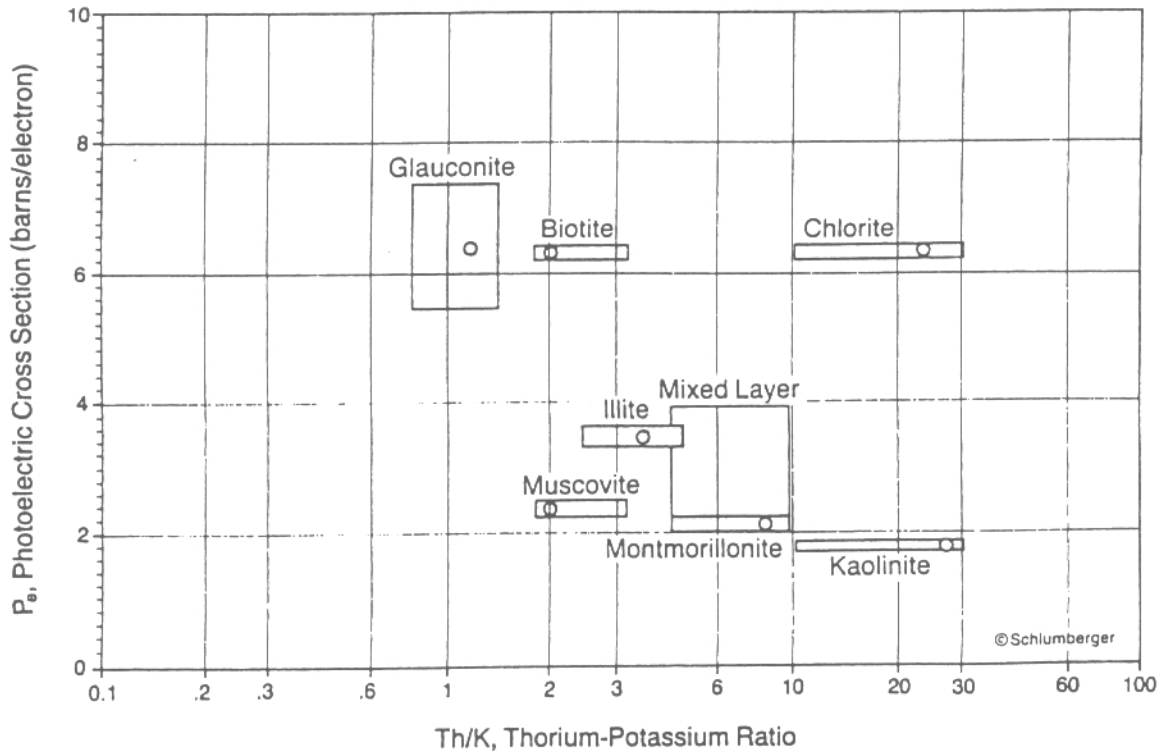
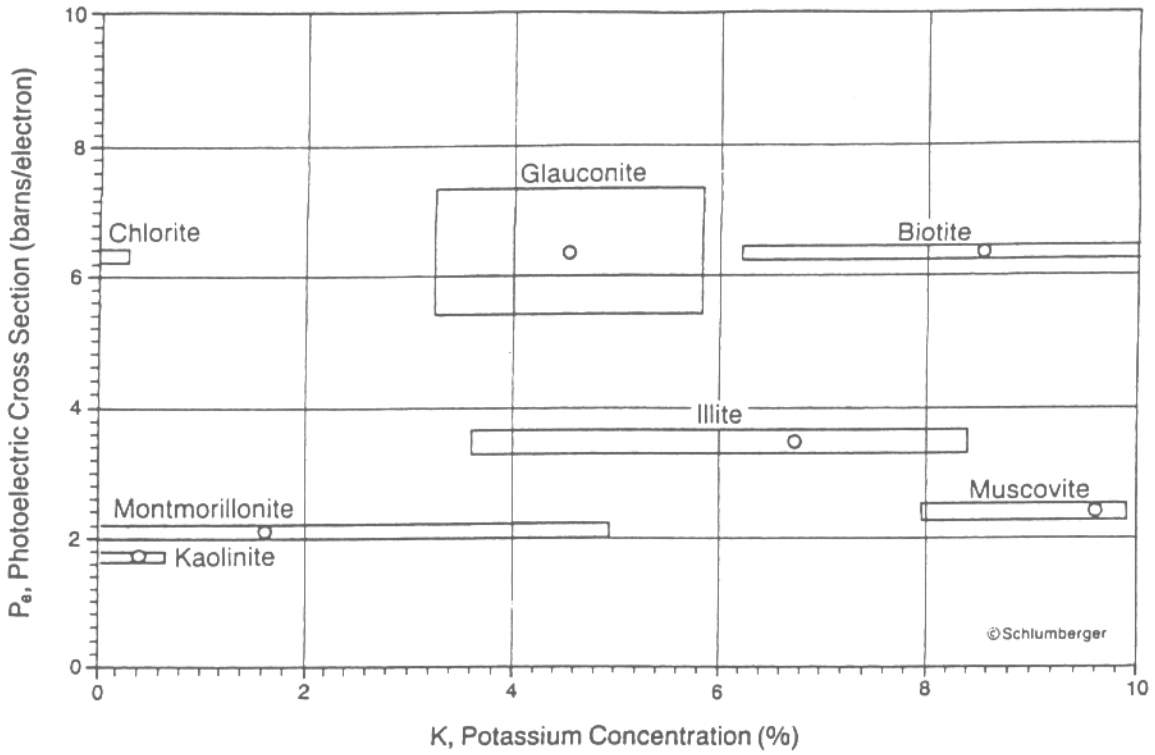


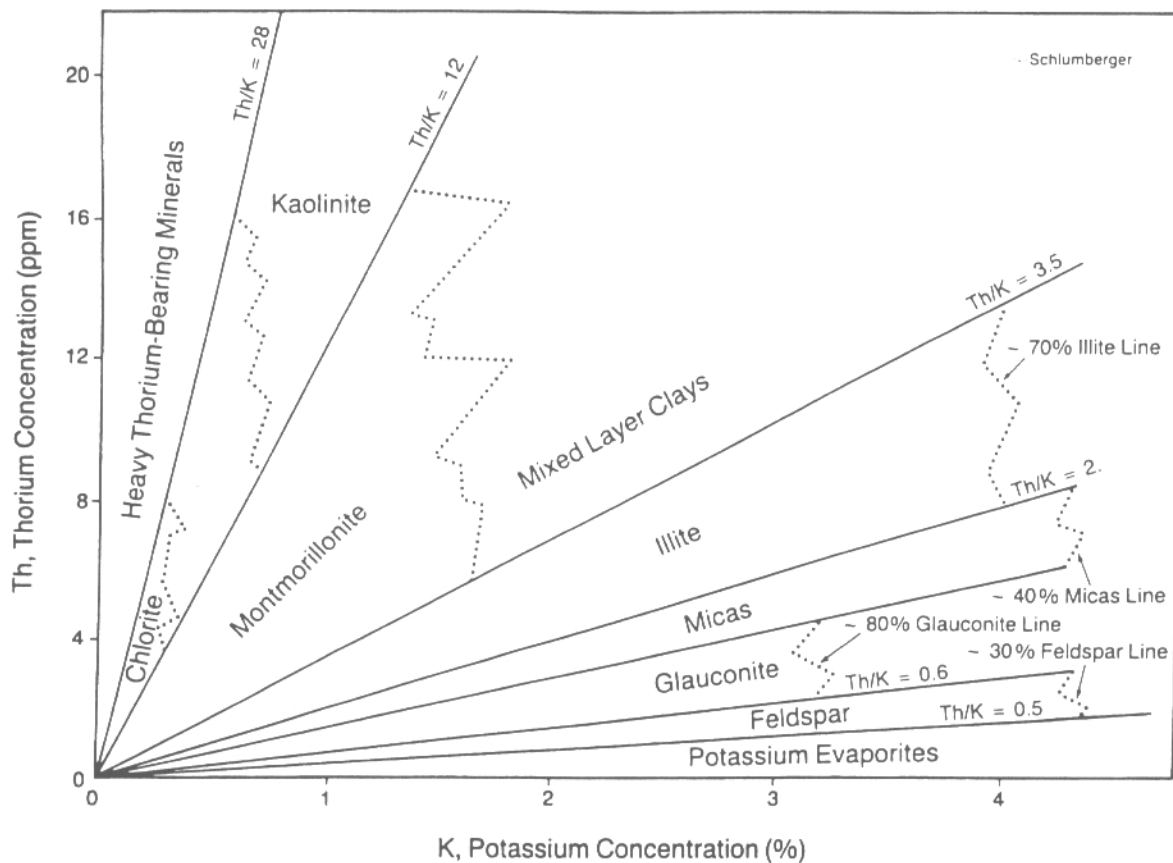
Figure 12b. UBI Borehole slip example. (Not from this well).



\*Mark of Schlumberger

CP-18

Figure 13. Mineral identification from Litho-Density Log and Natural Gamma Ray Spectrometry Log (Schlumberger Chart Book - 1984, Chart CP-18).



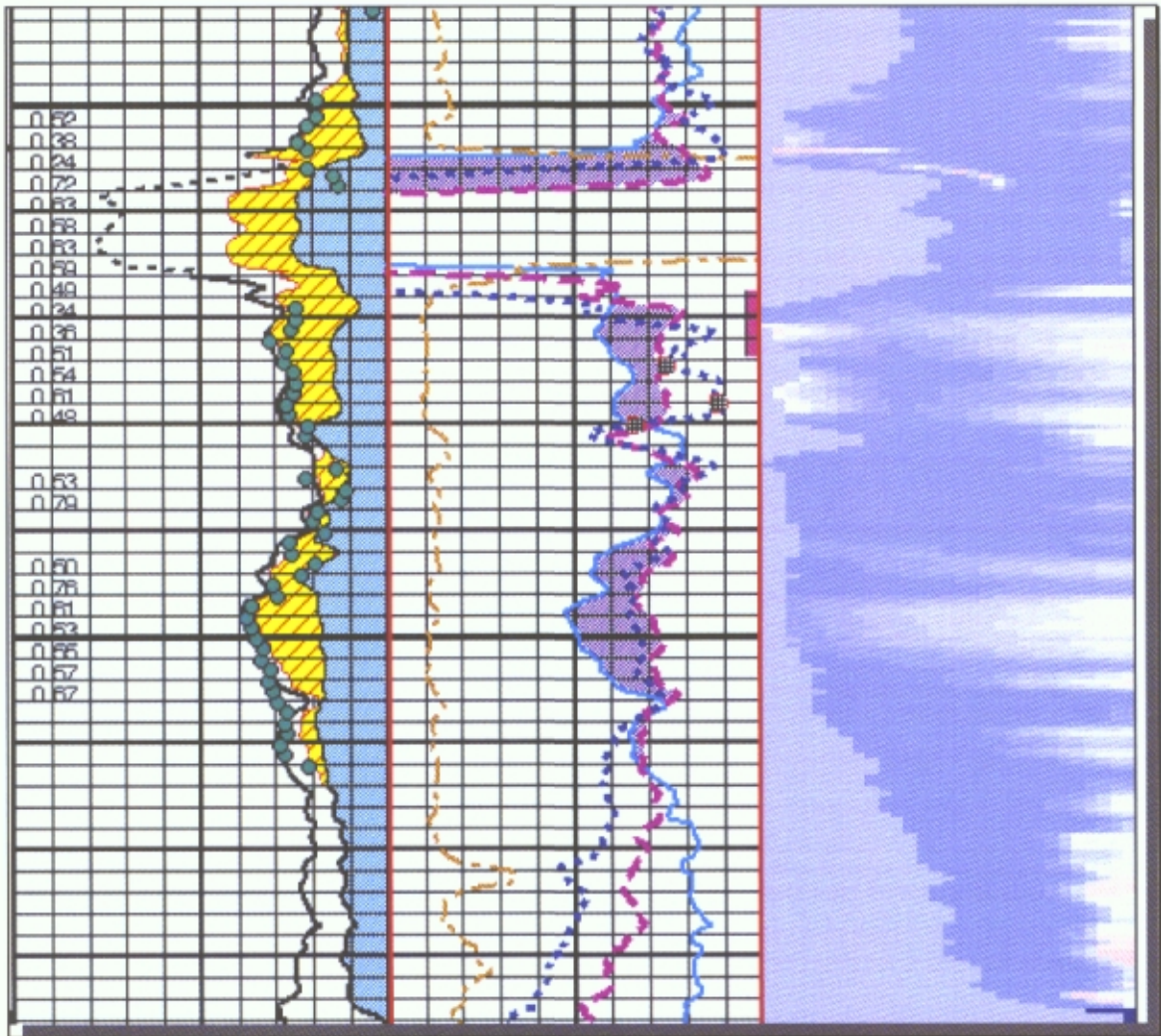
Charts (CP-18 and CP-19) provide insight into clay mineralogy using Natural Gamma Ray Spectrometry (NGS\*) and Litho-Density\* (LDT) measurements. Because the porosity and the composition of many clay minerals vary somewhat, the point at which clay minerals plot on these crossplots is not a unique point but a general area.

To use any of these charts, the appropriate parameters (after required environmental corrections) are crossplotted; their intersection provides insight into the mineralogy.

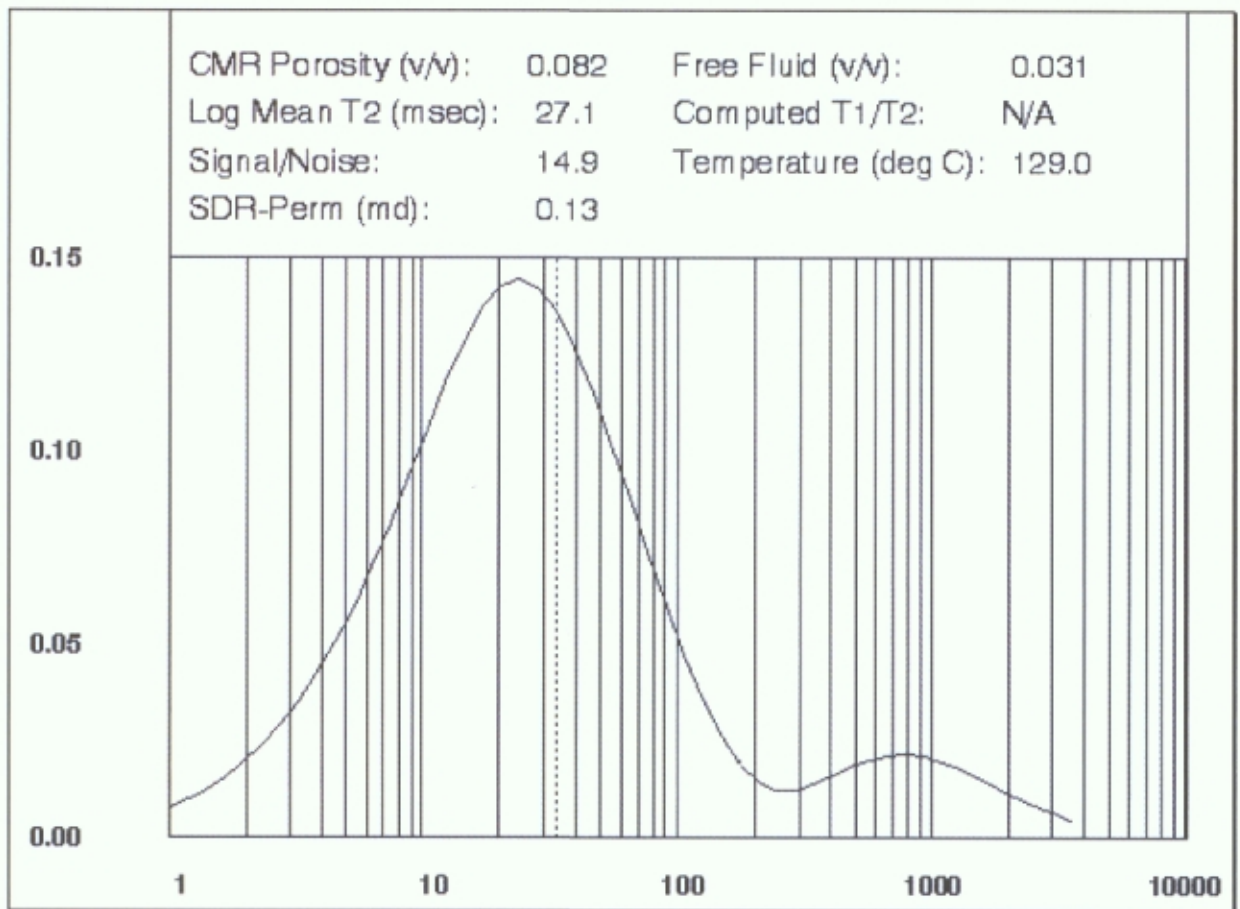
EXAMPLE:  $Th_{NGS_{cor}} = 10.6$  ppm,  $U_{NGS_{cor}} = 4.5$  ppm,  $K_{NGS_{cor}} = 3.9$  %  
 $P_c = 3.2$   
 Giving,  $Th/K = 10.6/3.9 = 2.7$

Thus, plotting these parameters on CP-18 and CP-19 suggests the clay mineral to be illite.

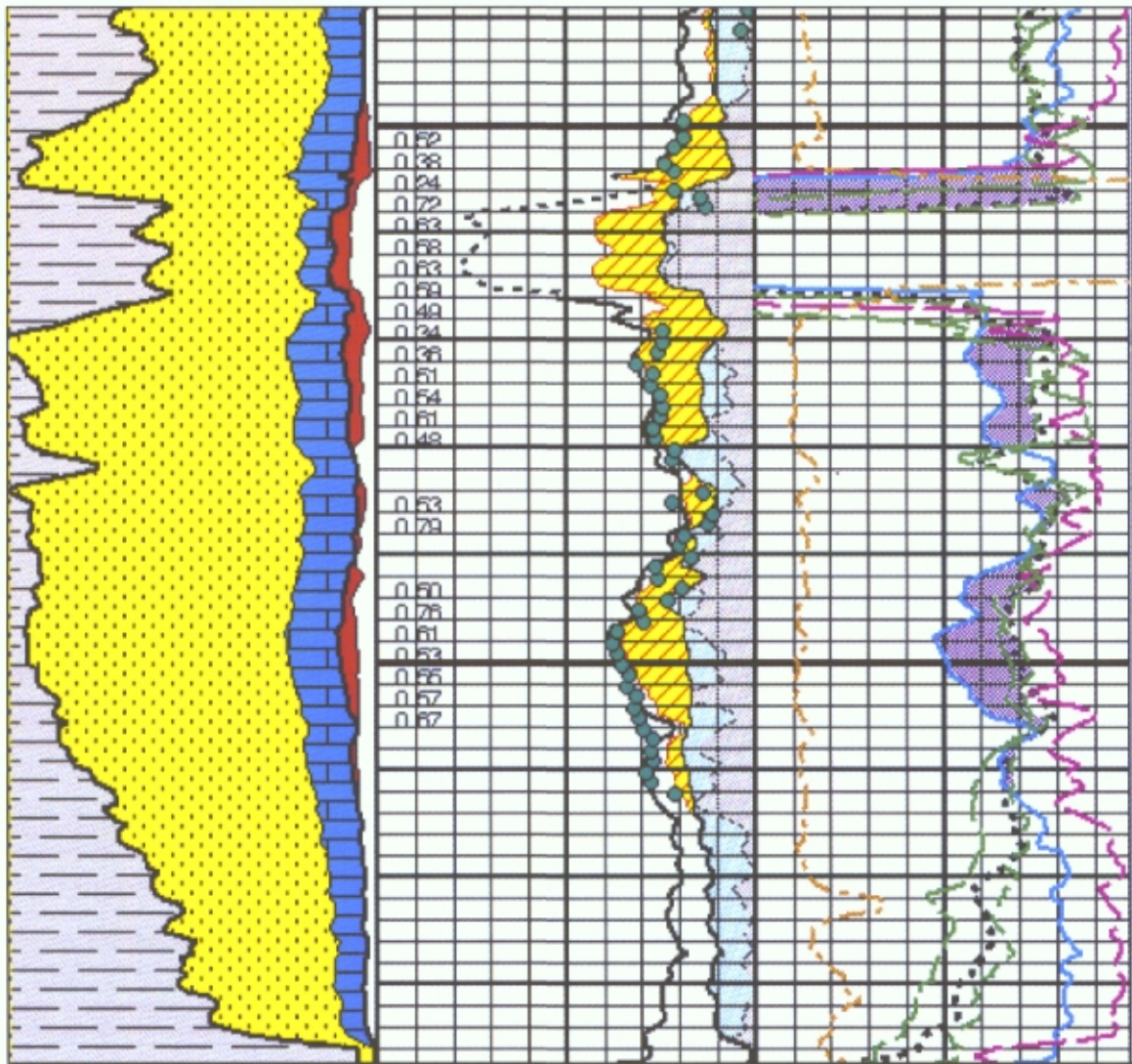
Figure 14. Mineral identification from Natural Gamma Ray Spectrometry (potassium) (Schlumberger Chart Book - 1984, Chart CP-19).



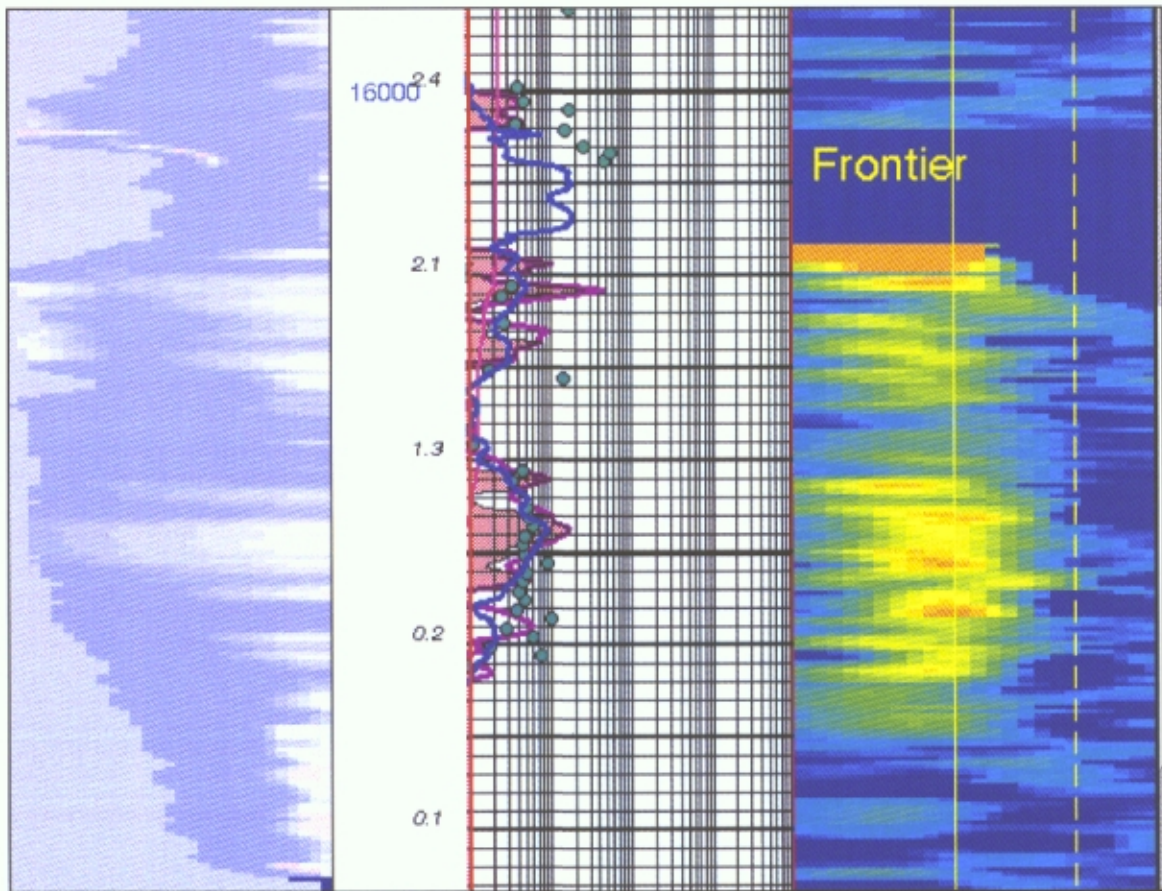
**Figure 15.** APS with LDT, CNL, and Flushing Estimates. Track 1 is the computed porosities 30%. Dashed area coding is the bulk volume water ( $\phi_{ie} \cdot S_w$ ). Small numbers are water saturations. Track 2 is the raw data (at bottom from left to right Pef, NPHI, APSC, and DPHI). Track 3 is the Neutron Gas Saturation Flushing estimate.



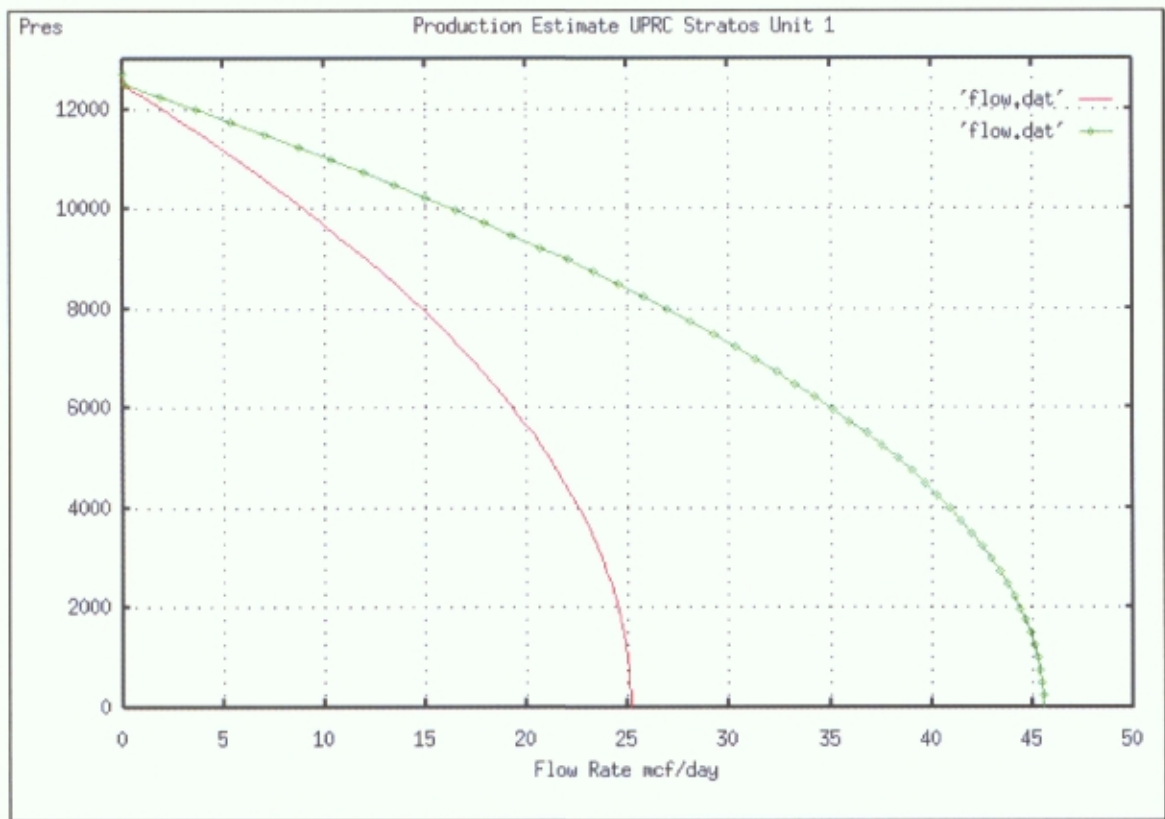
**Figure 16.** Station CMR at 16550 ft. Capillary bound porosity is left of the 33 line and moveable porosity is right of the line. Porosity is the area under the curve.



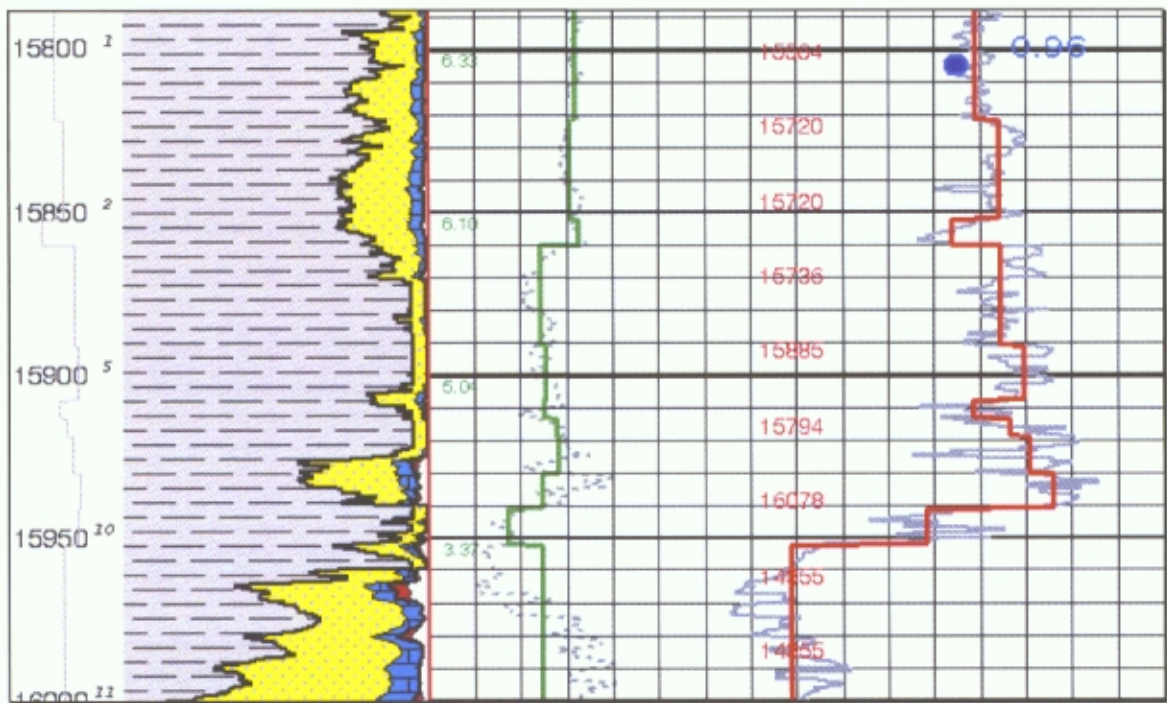
**Figure 17.** Porosity analysis with CMR. Track 1 is computed lithology. Track 2 is the computed porosity analysis (at the bottom of log from left to right, total porosity, effective porosity, bulk volume water, moveable fluid, and capillary bound fluid). Small numbers are water saturations. Track 3 is the raw data (at the bottom of the log from left to right PEF, NPFI, FPSC, APSC, DPHI, CMRP).



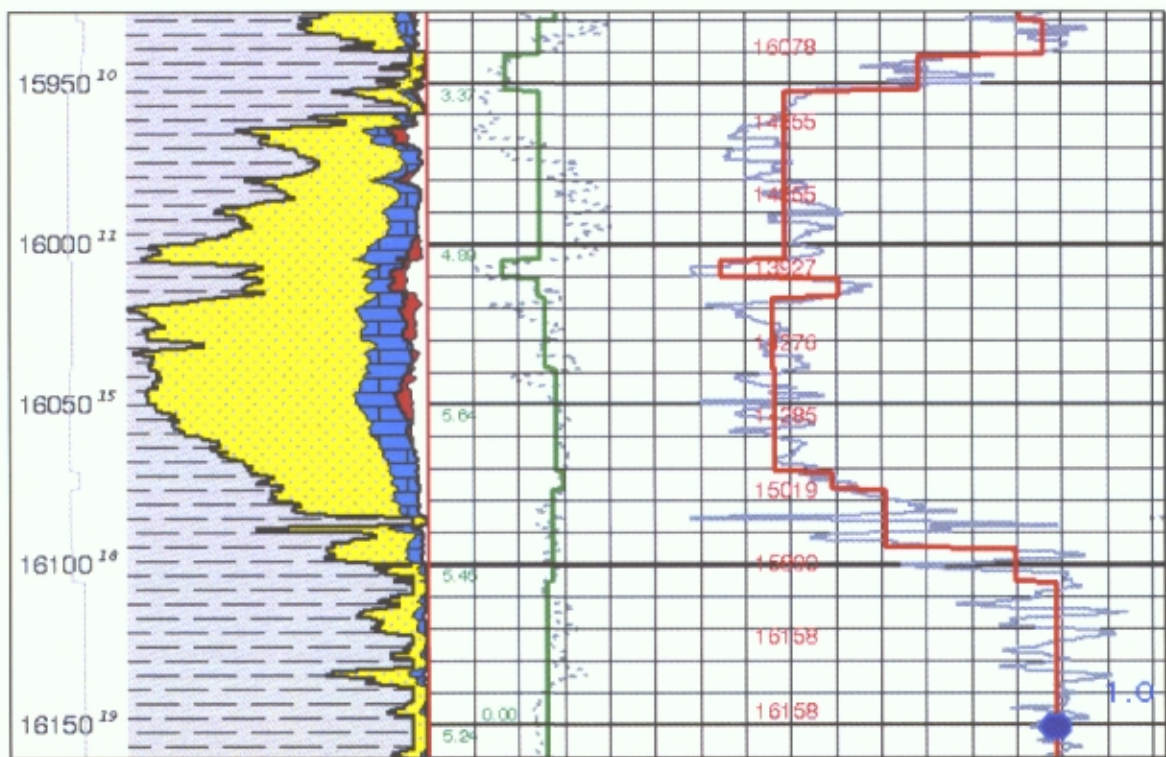
**Figure 18.** CMR T2 Distribution Track 1 is Neutron Flushing. Track 2 is the Permeability from 0.01 to 100 md, CMR, Neutron-Density, and Core. Track 3 is T2 Distribution. The solid line is 33 msec and the dashed line is at 200 msec. The small numbers in the depth track are integrated CMR permeability feet.



**Figure 19.** Benchmark estimates inside Performance line is a natural completion and the outside IPR line is after a moderate frac.



**Figure 20a - b.** Mechanical Properties Track 1 is lithology. Track 2 is Young's Modulus, raw and averaged, and Minimum far field stress, raw and averaged. Zone numbers are shown in the depth track.



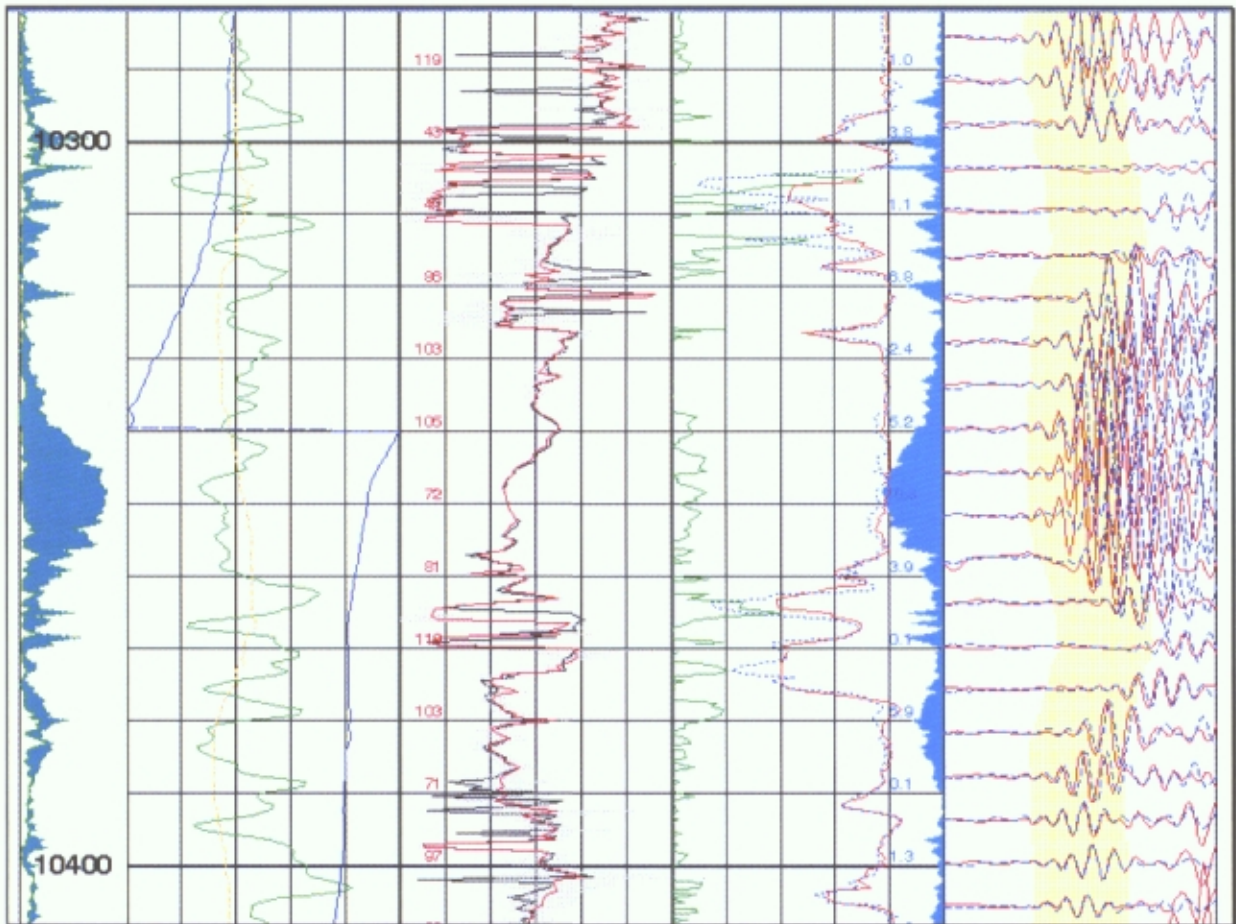


**Figure 21.** Example of BCR in Fractures. Depth track is min and max off-line energy. Track 1 is GR, Caliper, and Plaz. Track 2 is the fast shear azimuth. Track 3 is Fast and Slow Shear travel time. Track 4 is the fast and slow in-line waveforms.  
**(Not from this well).**



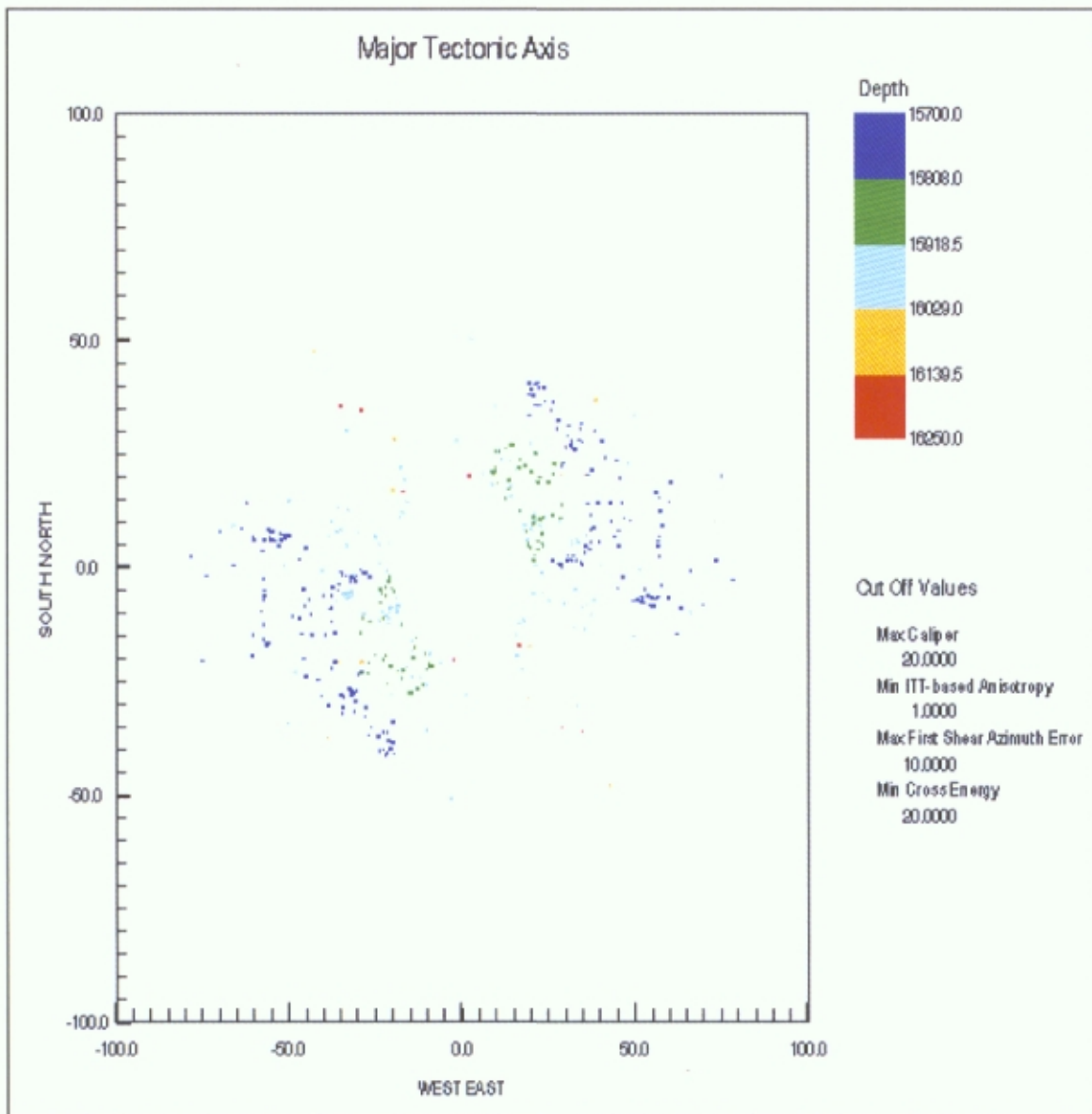


**Figure 23.** Anisotropy fast shear and stress direction from BCR.  
 No anisotropy means no strong anisotropy direction.